Luminescence could also be excited with reasonable efficiency by exciting in a broad band centered near 6500 Å. This undoubtedly corresponds to absorption into the $\Gamma_8(^2T_{2g})$ levels which could be seen in the absorption spectra reported by Dorain and also in our own samples. The measured lifetime was independent of the excitation wavelength. It is interesting to speculate on the nature of the excitation that leads to the luminescence particularly when the crystal is excited with ultraviolet light. In this case the excited state is at least 15 000 $cm^{-1}$ higher in energy than the nearest state that is within the $t_2^3$ configuration. This seems to be a rather large energy difference to be accounted for by a multiphonon relaxation unless there is considerable lattice relaxation within the excited state to which the transition initially occurs. Dorain and Wheeler give a value of 7% for the change in Re—Cl bond length for transitions to states of $t_{2g}^2e_g$ configuration. We can use this value to obtain a crude estimate of the decrease in energy of the lowest level of the $t_{2g}^2e_g$ configuration due to the change in crystal-field strength with dilation. A 7% change in bond length (assumed to be an expansion) leads to a decrease in crystal field of nearly 30%. Since in the region of large crystal fields the energy of the $^2T_{2g}$ levels is directly proportional to the strength of the field, this leads to a reduction in energy of this level likewise by about 30%. This is a decrease of some 10 000 $cm^{-1}$ to an energy only 5000 $cm^{-1}$ above the nearest $t_{2g}^3$ state. From this energy a relaxation via a configuration coordinate interaction to the $\Gamma_8(^2T_{2g})$ would be more probable eventually leading to population of the luminescent $\Gamma_7(^2T_{2g})$ level by additional multiphonon processes.

To our knowledge this constitutes the first observation of resolved sharp-line luminescence for a 5*d* ion. The observations are in excellent agreement with what could be expected based on the absorption measurements of Dorain and Wheeler. These suggest that sharp-line luminescence of the transition metals need not be restricted to elements of the first transition series but under appropriate conditions exist also for the 4*d* and 5*d* elements. Additional work along these lines is proceeding.

The original suggestion that the 5*d* ions might show sharp-line luminescence was made by M. de Wit to whom we are grateful for this as well as for his continuing interest and helpful criticisms. The authors benefited from many useful discussions with Dr. H. B. Bebb, Dr. R. K. Watts, and Dr. W. C. Holton. E. Ruthven and J. Pinnell are acknowledged for their assistance in preparing the crystals.

PHYSICAL REVIEW B VOLUME 1, NUMBER 5 1 MARCH 1970

# Field-Emission Studies of Electronic Energy Levels of Adsorbed Atoms

E. W. PLUMMER* AND R. D. YOUNG
*National Bureau of Standards, Washington, D. C. 20234*
(Received 13 June 1969)

The relative changes in the total energy distribution of field-emitted electrons upon adsorption of single atoms have been measured for adsorption of the alkaline-earth atoms (Ba, Sr, and Ca) on several crystal planes of tungsten. The expected perturbations of the energy distribution due to the tunneling resonance through an atomic "virtual level" at various positions relative to the Fermi surface and of various half-widths $\Gamma$ is demonstrated by a simple one-dimensional calculation. The measured energy-dependent structure in the current-enhancement factor due to the adsorbate has been interpreted in a tunneling-resonance model to yield the positions and shapes of the atomic "virtual levels." The ground-state $^1S$ $6s^2$ level of Ba is broadened to a half-width $\Gamma_S=0.75$ eV and shifted upward by $\Delta E^S=0.95$ eV. This causes it to overlap and mix with the first two excited states: a triplet $^3D$ $6s5d$ and a singlet $^1D$ $6s5d$. The observed $^3D$ and $^1D$ levels were not shifted and had a half-width $\Gamma_D=0.1$ eV. Similarly, the first excited state of Ca, a triplet $^3P$ $4s4p$, was shifted by $\Delta E^{3P}\approx0.4$ eV with a width $\Gamma_{3P}\approx0.3$ eV ($2\Gamma=$FWHM). The effect of the band structure of the substrate on tunneling resonance is discussed.

## I. INTRODUCTION

THE present knowledge of the interaction of atoms with surfaces has evolved from thermodynamic interpretation of a variety of experiments on increasingly clean and well-characterized surfaces. A rather recent shift to new and more sensitive experiments coupled with a spurt of quantum-theoretical calculations has signaled a turn toward quantum-mechanically oriented surface science. Furthermore, experimental techniques are now being developed and used which measure directly the quantum behavior of surfaces and adsorbate-surface interactions. In conjunction with recent theoretical studies, these experiments are expected to cast a new light on the fundamental behavior of surfaces and surface-atom interactions.

The scope of these experiments is evident from the examples which follow. Molecular vibrational levels of

* NRC-NBS Postdoctoral Research Associate at the National Bureau of Standards.

adsorbed molecules or of the adsorbed atom-substrate molecule have been observed in inelastically scattered electrons[1] and neutrons,[2] in inelastic tunneling of electrons in field emission,[3] in electron-impact desorption,[4] and in infrared adsorption.[5] Changes in electron-spin-resonance signals due to the presence of adsorbed gases have been detected.[6] Magnetic-field-induced surface quantum states have been observed in metals by microwave absorption techniques.[7] Finally, the subject which interests us most in this study is the position and shape of the electronic energy levels of adsorbates. They probably have been observed by Auger neutralization,[8] photoemission,[9] tunneling resonance of field-emitted electrons[10,11] and are anticipated in experiments involving inelastically scattered electrons.[12] These experiments have all used or developed sophisticated experimental techniques and apparatus to accomplish their objectives. There is a clear trend among those now entering the field of surface science to exploit these new techniques and to interpret them in terms of quantum-mechanical models. The information thus gained will be particularly useful in extending the understanding and interpretation of the body of existing knowledge in surface science.

The theoretical picture has developed just as rapidly in the last few years. It is difficult now to say with any confidence, as Gomer[13] could in his review, that the experimental side looks somewhat brighter than the theoretical. To illustrate the theoretical progress, consider the calculations concerning atomic energy levels of adsorbates on metal surfaces. Schmidt and Gomer[14] pointed the way to understanding electropositive adsorption in terms of the position and width of the atomic band in the adsorbate relative to the Fermi surface of the metal. Gadzuk[15] and Bennett and Falicov[16] followed with detailed theoretical calculations of the position and lifetime broadening of the virtual-electron energy level (atomic band) as a function of the relevant physical parameters. Then Gadzuk[17] combined the calculations of the position and width of the atomic band with a previous calculation of the screening of an impurity at the surface to calculate the effective charge on the adsorbate, its screening length, and consequently its dipole moment. The agreement between his theory and experiments for alkali adsorption on several faces of several metals is remarable.[17] The fact that experimental data relating directly to the shape and position of the atomic bands are almost nonexistent indicates the state of the art experimentally in this field. Yet the theoretical work has clearly shown that, at least for electropositive adsorbates, the interaction of the adsorbed atom with the surface can be characterized in terms of the shift and broadening of the atomic level in the atom. We hope to demonstrate here that this information is obtained directly from energy analysis of electrons field-emitted through adsorbed atoms.

The history of the field-emission microscope, which has proved to be one of the most powerful surface tools,[18] exemplifies the general trend in surface research discussed above. The first experiments consisted in visually (or photographically) observing the qualitative changes in the emission pattern or measuring the changes in the total current change upon absorption. With the development of the probe-hole tube,[19] the changes in the field-emission current could be measured from individual crystal planes. This development opened another dimension to adsorption studies in field emission, and tremendously important work concerning the perplexing problem of the effect of surface crystallography was conducted. Yet up to this stage of the development of the field-emission microscope the experiments were usually interpreted in terms of thermodynamic quantities such as work function change, polarization, etc. Duke and Alferieff[20] (DA) pointed out that these quantities are not necessarily sufficient to explain the effects of the adsorbate on field emission, because the adsorbate changes the qualitative shape of the potential barrier seen by the tunneling electrons and because the adsorbate can act as an energy-momentum source (sink) for the tunneling electrons. This fresh approach to an old problem by DA illustrates the quantum-mechanical effects of the potential due to the adsorbed atom on the energy distribution of the tunneling electrons and indicated a new direction that experimental field-emission work could now take. The energy distribution of field-emitted electrons is inherently more sensitive to the potential near the surface than

[1] F. M. Propst and T. C. Piper, J. Vac. Sci. Technol. **4**, 53 (1967).
[2] H. Boutin and H. Prask, Surface Sci. **2**, 261 (1964).
[3] L. W. Swanson, Proceedings of the Twenty-Ninth Conference on Physical Electronics, 1969 (unpublished).
[4] T. E. Madey and J. T. Yates, J. Chem. Phys. **51**, 1264 (1969).
[5] J. F. Harrod, R. W. Roberts, and E. F. Rissman, J. Phys. Chem. **71**, 343 (1967).
[6] M. F. Chung and D. Haneman, J. Appl. Phys. **37**, 1879 (1966).
[7] J. F. Koch, Phys. Rev. **164**, 618 (1967).
[8] H. D. Hagstrum and G. E. Becker, Phys. Rev. Letters **22**, 1054 (1969); Proceedings of the Twenty Ninth Conference on Physical Electronics, 1969 (unpublished).
[9] B. J. Waclawski, L. R. Hughey, and R. P. Madden, Appl. Phys. Letters **10**, 305 (1967).
[10] H. E. Clark and R. D. Young, Surface Sci. **12**, 385 (1968).
[11] E. W. Plummer, J. W. Gadzuk, and R. D. Young, Solid State Commun. **7**, 487 (1969).
[12] C. J. Powell (private communication).
[13] R. Gomer, *Fundamentals of Gas-Surface Interactions* (Academic Press Inc., New York, 1967).
[14] L. Schmidt and R. Gomer, J. Chem. Phys. **42**, 3573 (1965).
[15] J. W. Gadzuk, Surface Sci. **6**, 133 (1967).
[16] A. J. Bennett and L. M. Falicov, Phys. Rev. **151**, 512 (1966).
[17] J. W. Gadzuk, Proceedings of the Fourth International Materials Symposium on the Structure and Chemistry of Solid Surfaces, 1968 (unpublished).
[18] E. W. Müller, Ann. Rev. Phys. Chem. **18**, 35 (1967); G. Ehrlich, *ibid*, **17**, 295 (1966); R. Gomer, *Field Emission and Field Ionization* (Harvard University Press, Cambridge, Mass., 1961).
[19] E. W. Müller, J. Appl. Phys. **26**, 732 (1955).
[20] C. B. Duke and M. E. Alferieff, J. Chem. Phys. **46**, 923 (1967).

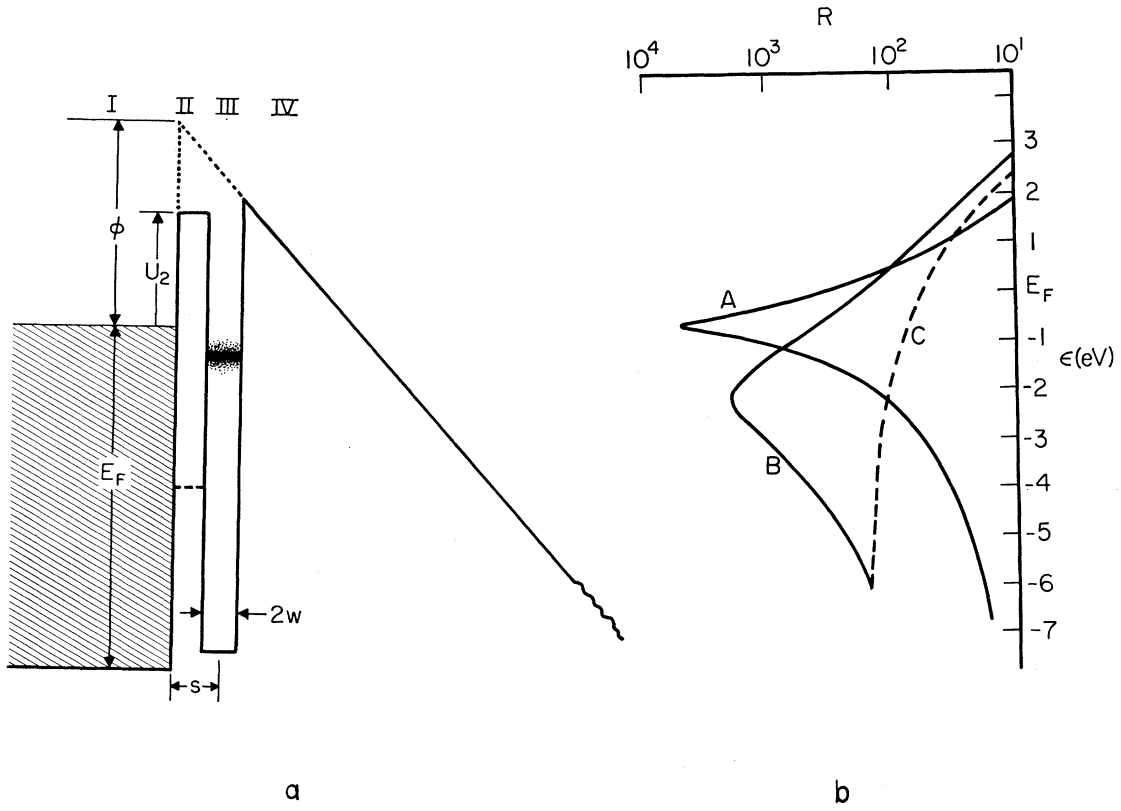


FIG. 1. (a) One-dimensional potential model for the metal (region I) and the adsorbate (region III), in the presence of an applied field. The width $2w$ and depth of the potential well in region III have been chosen so that the first bound state is at $\epsilon = -0.7$ eV (shaded area in region III). (b) Calculated tunneling-enhancement factor $R$ for the potential model in (a). Curve A is for the potential drawn by the solid lines in (a). Curve B is the enhancement factor when the height of the barrier in region II is reduced to the dashed line at $\epsilon = -3.5$ eV. Curve C is the nonresonant contribution to the tunneling in case A.

the current density which is an integral over all energies. Preliminary results using this technique to study adsorption[3,10,11] have been very encouraging.

The DA model demonstrated that resonance transmission of tunneling electrons will occur in field emission when the incident electrons from within the metal have the same energy as a virtual level (atomic band) in the adsorbed atom. The resonance is due to the interference of the de Broglie waves, in analogy with the phenomena observed in the optical interferometer. This phenomenon is discussed in nearly any quantum-mechanics textbook,[21] and the case of unequal barriers has been discussed by Iogansen[22] within the context of the WKB approximation.

## II. CALCULATION OF TUNNELING RESONANCE

The salient features of the effect of resonance transmission of tunneling electrons on the energy distribution of field-emitted electrons can be illustrated by the use of the simple one-dimensional model potential shown in Fig. 1(a).[20] Region I is the free-electron metal with a Fermi surface at $E_F$ and a work function $\varphi$. The atomic potential of the adsorbate in the presence of the applied field is represented by a one-dimensional square well (region III). The tunneling probability through this compound barrier was calculated in the same manner as used by DA[20]; i.e., by matching the logarithmic derivative of the wave function at each barrier. The problem was simplified by calculating the tunneling probability through region IV by the WKB method to avoid the use of Airy functions. This compromise will not change any of the basic features since region IV is thick compared to the wavelength of the electron and the width of the other barriers. Utilizing this simple model we can extend the DA calculations to illustrate the effect on the energy distribution of adsorbates with energy levels (bands) of various shapes and positions. Consequently, we are able to predict qualitatively what the experimentalist should expect to see for different types of adsorbates.

The enhanced-resonance factor $R$ is defined as the ratio of the tunneling probability of an electron through

[21] E. Merzbacher, *Quantum Mechanics* (John Wiley & Sons, Inc., New York, 1961), p. 124; D. Bohm, *Quantum Theory* (Prentice-Hall, Inc., Englewood Cliffs, N. J., 1951).

[22] L. V. Iogansen, Zh. Eksperim. i Teor. Fiz. **45**, 207 (1963); **47**, 270 (1964) [English transls.: Soviet Phys.—JETP **18**, 146 (1964); **20**, 180 (1965)].

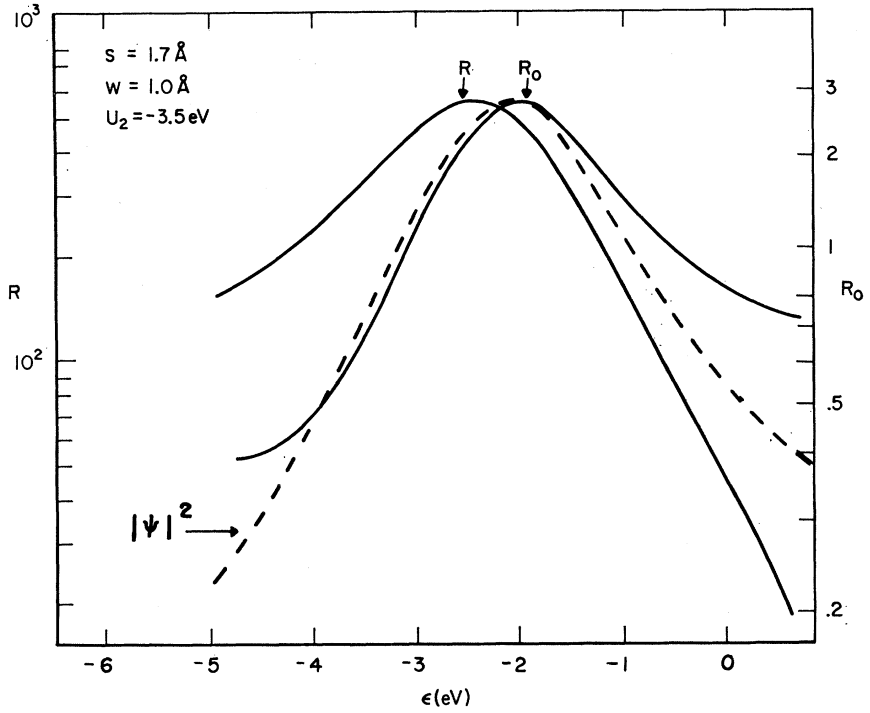


FIG. 2. Calculated tunneling-enhancement factor $R$ for a potential well 2 Å wide, 8 eV deep, and 1.7 Å from the surface. $R_0$ is the true resonance factor, which is the enhanced-tunneling factor $R$ with the nonresonant contribution divided out, while $|\psi|^2$ is the actual wave-function probability in region III. Note that the peak position in the enhanced-tunneling factor can be shifted due to the nonresonant contribution. The peak heights have been normalized and $\epsilon = E - E_F$.

the barrier with the atomic potential present (region III) with respect to the tunneling with the atomic potential missing [dotted line in Fig. 1(a)]. Curve A of Fig. 1(b) shows the calculated enhanced-tunneling factor for the potential shown in Fig. 1(a) by the solid line, where the depth and width of the well were chosen so that the first bound state is 0.7 eV below the Fermi surface ($\epsilon = -0.7$). The simple physical properties of the interaction of the atom with the surface can be demonstrated with this model. As the depth or width of the potential well is varied so that the bound state moves up or down, the resulting enhancement curve follows the motion of the band. When the width or height of region II is increased or decreased, the width of the enhanced-tunneling curve decreases or increases, respectively. This is a consequence of the lifetime broadening of the atomic state which increases as the barrier is reduced and decreases as the barrier becomes larger, i.e., the interaction of the atomic state with the metal respectively increases and decreases. Therefore, having determined the relationship between the shape of the enhanced-tunneling curve and the line shape of the atomic band, we can determine the position and width of the atomic band from the enhanced-tunneling curves obtained from the measurement of the energy distribution of field-emitted electrons through an absorbed atom. This is a subject which has been theoretically investigated in detail by Gadzuk.[23] We will demonstrate within the context of the DA model the qualitative differences between the shape of the enhanced-tunneling factor and the atomic band.

[23] J. W. Gadzuk, following paper, Phys. Rev. B 1, 2110 (1970.)

Since the details of the potential barrier between the metal and the atom (region II) are relatively unknown, it is important to demonstrate that the height of this barrier is not fundamental in establishing resonance. Curve B of Fig. 1(b) is for a barrier in region II of height less than the resonance energy (dashed line 3.5 eV below the Fermi surface in region II). Resonance still occurs in analogy with the well-known Ramsauer effect in electron scattering. The position and shape of the enhanced-resonance curve have changed as a consequence of the change in the virtual level in the atom. The drop in energy can be calculated from the decrease in the barrier height[24] and the lifetime broadening of the state increases also as a consequence of the decrease in the barrier (strong interaction with the metal).

The shape of the enhanced-resonance curve is not identical to the shape of the wave-function probability in the region of the potential well as a result of the nonresonant increase in the tunneling and to interference terms.[23] Curve C of Fig. 1(b) is the nonresonant increase in the tunneling corresponding to curve A due to cutting a chunk out of the original barrier. In Fig. 2 we plot the calculated enhanced-tunneling factor $R$ and the truly resonant contribution $R_0$, where $R_0$ is the enhanced-tunneling factor through the barrier with the nonresonant part divided out (curve A divided by C in Fig. 16). The dashed curve in Fig. 2 is the actual wave-function probability $|\psi|^2$ in the region of the atomic

[24] L. D. Landau and E. M. Lifshitz, *Quantum Mechanics* (Addison-Wesley Publishing Co., Inc., Reading, Mass., 1958), p. 63.

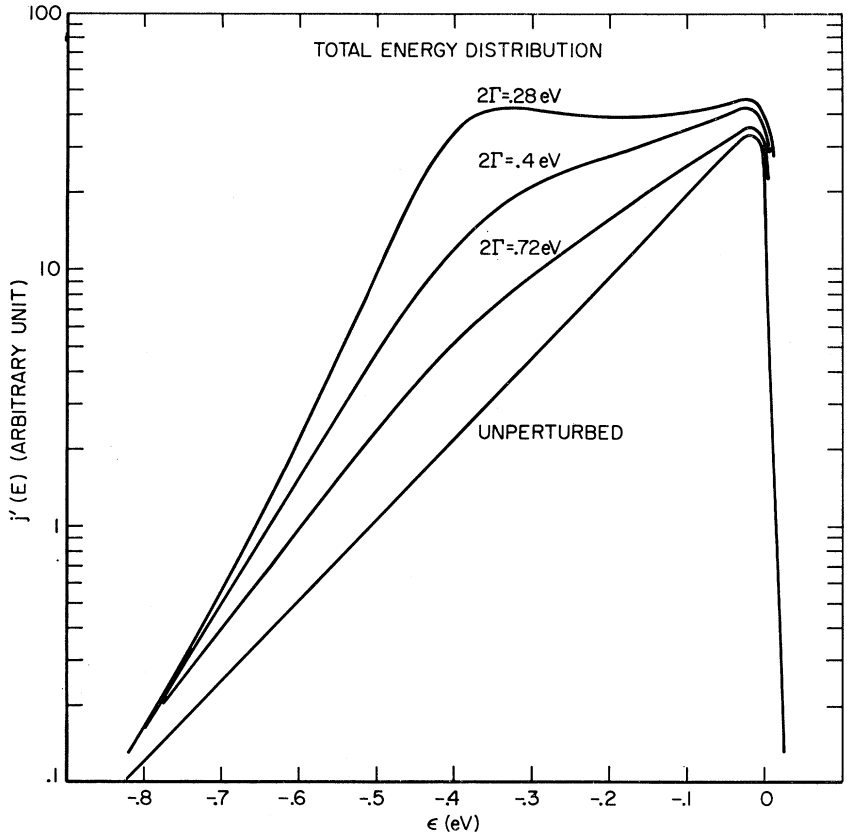


FIG. 3. Calculated total energy distributions through an adsorbed atom with an energy level 0.4 eV below the Fermi surface with various half-widths Γ. The width of the band was calculated from the true resonant factor $R_0$ (Fig. 2). All of the curves are normalized at the Fermi surface where $\epsilon = E - E_F$ and ($2\Gamma$ = FWHM).

potential (region III). The small difference between the resonant curve $R_0$ and $|\psi|^2$ is due to the interference between the direct and resonance tunneling channels.[23] The deviation of the maximum for both the enhanced-resonance factor $R$ and the true tunneling-resonance factor $R_0$ from the maximum in $|\psi|^2$ was found to be proportional to the square of the half-width of the $|\psi|^2$ curve. The separation between the maximum was 0.3 and 0.06 eV for the $R$ and $R_0$ curves, respectively, for an atomic band of half-width 1 eV.

At this point, the results of this exact calculation using the DA[20] model coincide with the more physically satisfying formulation of Gadzuk.[23] The two calculations must yield the same enhancement factors because they both use the same potential model for the metal and adsorbate. In principle, we should use a momentum-dependent potential for the adsorbed atom; but since the energy levels of the adsorbed atom are broadened owing to the interaction with the metal surface, there should not be a dramatic energy dependence of the atomic potential over an energy range compared to the width of the energy levels. Obviously, an electron with energy far above or below an atomic energy level will feel a different adsorbate potential. What is appealing about Gadzuk's calculation is that (a) it indicates the physical origin of the differences between the curves in Fig. 2; (b) it has been extended to include adsorbates with different angular momentum states; and (c) the model enables us to determine the shape of the virtual level from the experimentally accessible enhancement factor ($|\psi|^2$ from curve R in Fig. 2).

In Fig. 3, we have calculated what the actual energy distribution through an adsorbate with an atomic band 0.4 eV below the Fermi surface ($\epsilon = -0.4$) will look like for various widths, where $2\Gamma$ is the full width at half-maximum (FWHM) of the line shape of the electron density in the atomic band. These curves indicate that pronounced structure should not be expected for $s$ bands in atoms adsorbed on the surface since these bands will probably be wider than 0.7 eV.[15,16] Also, the present technique used for energy analysis is the retarding-potential method, whose working range is less than 1.0 eV below the Fermi surface. Therefore, the broad bands expected for aklali adsorption[17] will only perturb the logarithm of the slope of the energy distribution, with little or no detailed structure present in this limited energy range.

The are three obvious ways of creating narrow states or sharp resonances. The first is to move the atom away from the surface.[15,16] This could be accomplished by depositing a complex molecule on the surface, but the relevant information about the surface adatom interaction would be lost and the resonance spectrum is likely to be very comeplx because of the other atoms

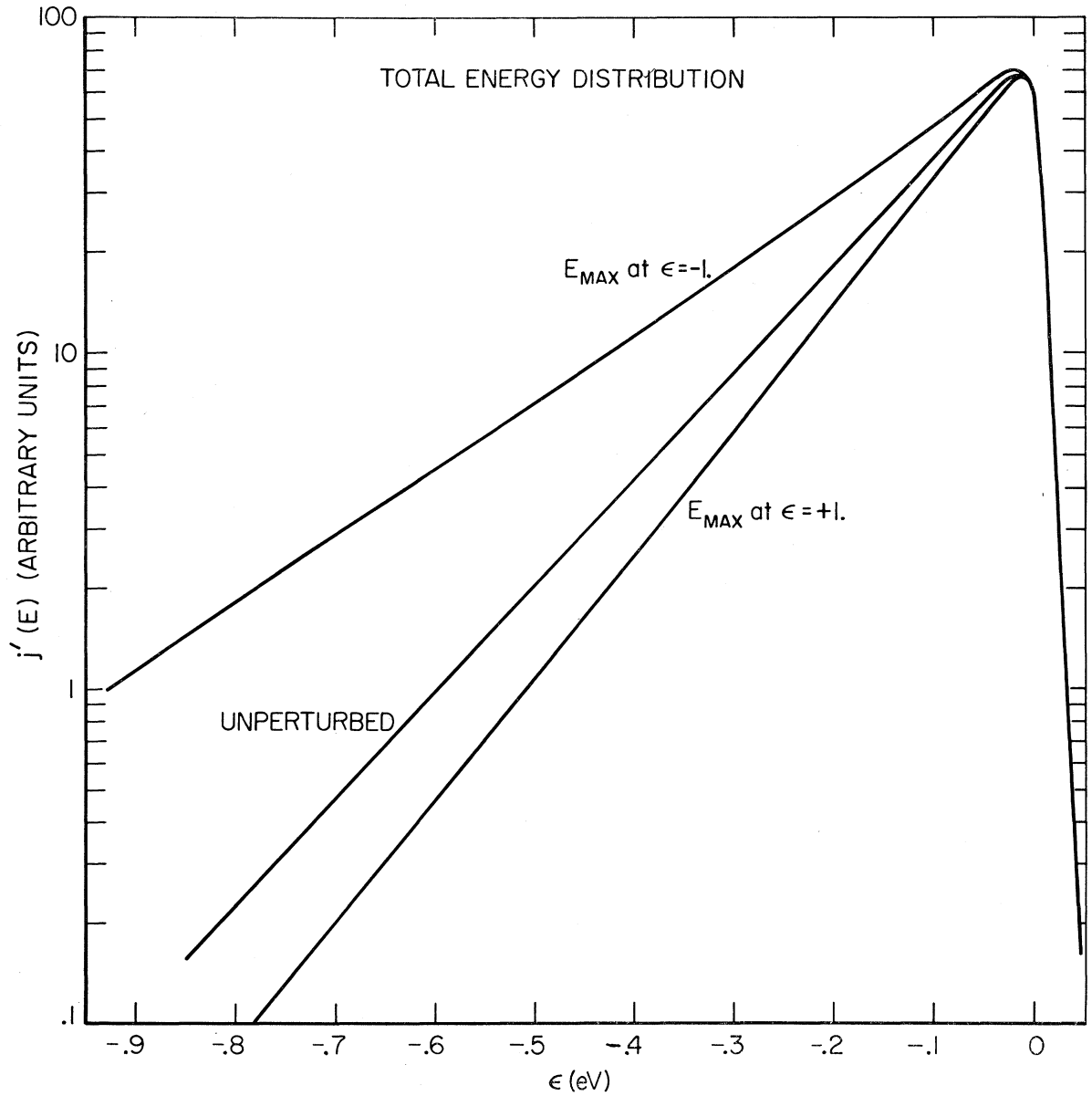


FIG. 4. Calculated effect on the total energy distribution for a broad band 1 eV above and below the Fermi surface; $\epsilon=1$ eV and surface; $\epsilon=1$ eV and $\epsilon=-1$ eV, respectively ($\epsilon=E-E_F$). The unperturbed curve is the total energy distribution before adsorption.

in the molecule and the various configurations the molecule can have on the surface.[3] The second method is to look at higher-angular-momentum states of an adsorbed atom. The effect of the angular momentum barrier $[l(l+1)/r^2]$ is to increase the barrier between the atomic state and the surface and consequently reduce the width of the state.[23] In other words, the effective extent of the wave function of the atom is reduced, its overlap with the metal wave function decreases, and consequently the width of the higher-angular-momentum state is less. For example, Cooper[25] has calculated that the radial part of the wave function for the 6*s* state is about twice as extended as the first-excited 5*d* state in Ba even when the *d* state is at a higher energy. The third and final way to create a narrow atomic band is to move the energy level in the atom far below the Fermi surface. But this state would not be observable, at least with a retarding-potential energy analyzer.

In Fig. 3, the position of the band was chosen so that the peak would be in the middle of the energy distribution. In Fig. 4, the effect of a broad band [0.7 eV FWHM] 1.0 eV above and below the Fermi surface is shown along with the unperturbed energy

[25] J. W. Cooper (private communication).

distribution. It is obvious that the atomic band affects the energy distribution even when the peak is 1 eV away, but there is no noticeable structure. When the level is above the Fermi surface ($\epsilon=1$) the logarithm of the slope of the energy distribution is larger than the unperturbed curve, and when the level is below the Fermi surface the logarithm of the slope is decreased. In fact a band of half-width $\Gamma$ can cause a 10% change in the logarithm of the slope of the energy distribution when the peak in the energy distribution is approximately $1/\Gamma$ away from the Fermi surface (for $\Gamma \leq 1.5$ eV). The logarithm of the slope of the energy distribution has been combined with the slope of the Fowler-Nordheim (FN) equation to obtain work functions for clean surfaces.[26,27] The strong influence of the position of the band on the energy-distribution slope indicates that this technique is not applicable to low-coverage adsorption systems. At higher coverages of metallic adsorbates the band probably broadens sufficiently so that there would be little perturbation of the energy distribution.

Figures 3 and 4 have illustrated that we should not expect any pronounced structure in the energy distribution for adsorbates like the alkali metals, because these one-electron adsorbates will have realtively wide bands.[17] For this reason we have chosen to look at the alkaline-earth atoms adsorbed on tungsten, in hope that they might exist on the surface in a higher-angular-momentum state with more detailed structure.

There have been several observations in field emission which are probably caused by tunneling resonance. (1) Dobretsov[28] employed the concept of enhanced tunneling to explain the structure in the energy distribution electrons emitted from tungsten through a thin layer of germanium.[29] (2) The classical case is nitrogen adsorption on tungsten.[30] The current density decreases while the slope of the FN plot also decreases, which is a contradiction of predicted FN behavior. Van Oostrom[31] observed that the half-width of the energy distribution from the (114) plane increased after adsorption of nitrogen at 78°K. We have also measured the slope of the energy distribution from the (013) after equivalent treatment of nitrogen and found that it decreased, which causes a larger half-width. DA[20] have shown these results can be explained in the tunneling-resonance model if the adsorbate has an energy level far below the Fermi surface. (3) Clark and Young[10] found that a strontium atom deposited on an oxygen-covered tungsten tip caused a current-density increase accompanied by an increase in the logarithm of the slope of the energy distributlon. They showed that this is inconsistent with the FN model and attributed it to a wide band in the strontium atom above the Fermi surface. We have shown in a recent letter[11] how one can use this change in the logarithm of the slope of the energy distribution upon adsorption of zirconium on different work function surfaces of tungsten to map out the rough shape of the atomic band in zirconium.

A much more critical question is what effect the distortion of the energy distribution due to an atomic band of an adsorbate will have on the slope of the FN plot. Fortunately, it is relatively easy to show that in most cases the slope of the FN plot will be unperturbed.[20] This results from the fact that the slope of the FN plot depends basically upon the tunneling probability at the Fermi surface,[32] and in general the perturbation of the energy distribution will manifest itself in current-density changes (preexponential term). But the slope of the FN equation can be affected if a narrow band is swept through the Fermi surface as the field is changed,[20] that is, if the band is positioned near the Fermi surface and has a width nearly as small as the shift in energy caused by the field change, or if a narrow band lies slightly below the Fermi surface such that the enhanced tunneling through the band causes an appreciable fraction of the total current to be emitted at the resonant energy instead of at the Fermi surface. This effect has been observed for $\chi$ nitrogen, where a sharp energy level ($\Gamma \sim 0.2$ eV) was observed near the Fermi surface,[11] and phthalocyanine[3] on tungsten.

In the previous discussion we have ignored two important physical facts. The first is that in field emission we measure a total energy distribution,[32] while the tunneling-resonance calculations are for normal energy (one dimensional). The tunneling through the barrier is basically a normal-energy problem while resonance is inherently a total-energy phenomenon. A truly total-energy calculation has not been done, but Gadzuk[23] has shown how in principle it could be carried out. If the atomic well is very small compared to the thickness of the total barrier, then the one-dimensional approach is probably a good fisrt approximation. The second effect we have ignored is the non-free-electron behavior of the electrons in the metal. The incident electrons from within the metal will deviate from plane waves and their character will be energy- and directional-dependent. The effect of band structure on field emission from clean surfaces is not fully understood at the present time[27,33,34] and its manifestations on the enhanced tunneling is unknown. Two examples will be shown later which are probably due to band-structure effects.

[26] R. D. Young and H. E. Clark, Appl. Phys. Letters **9**, 265 (1966).
[27] L. W. Swanson and L. C. Crouser, Phys. Rev. **163**, 622 (1967).
[28] L. N. Dobretsov, Fiz. Tverd. Tela **7**, 3200 (1965) [English transl.: Soviet Phys.—Solid State **7**, 2589 (1966)].
[29] I. L. Sokol'skaya and N. V. Mileshkima, Fiz. Tverd. Tela **3**, 3389 (1961); **6**, 1369 (1964); **7**, 1043 (1965) [English transls.: Soviet Phys.—Solid State **3**, 2460 (1962); **6**, 11401 (1964); **7**, 838 (1965)]; N. V. Mileshkina and I. L. Sokol'skaya, *ibid.* **5**, 2501 (1963) [English transl.: *ibid.* **5**, 1826 (1964)].
[30] G. Ehrlich and F. G. Hudda, J. Chem. Phys. **35**, 1421 (1961).
[31] A. van Oostrom, Philips Res. Rept. Suppl. **11**, 102 (1966).
[32] R. D. Young, Phys. Rev. **113**, 110 (1959).
[33] L. W. Swanson and L. C. Crouser, Phys. Rev. Letters **16**, 389 (1966); **19**, 1179 (1967).
[34] J. W. Gadzuk, Phys. Rev. **182**, 416 (1969).

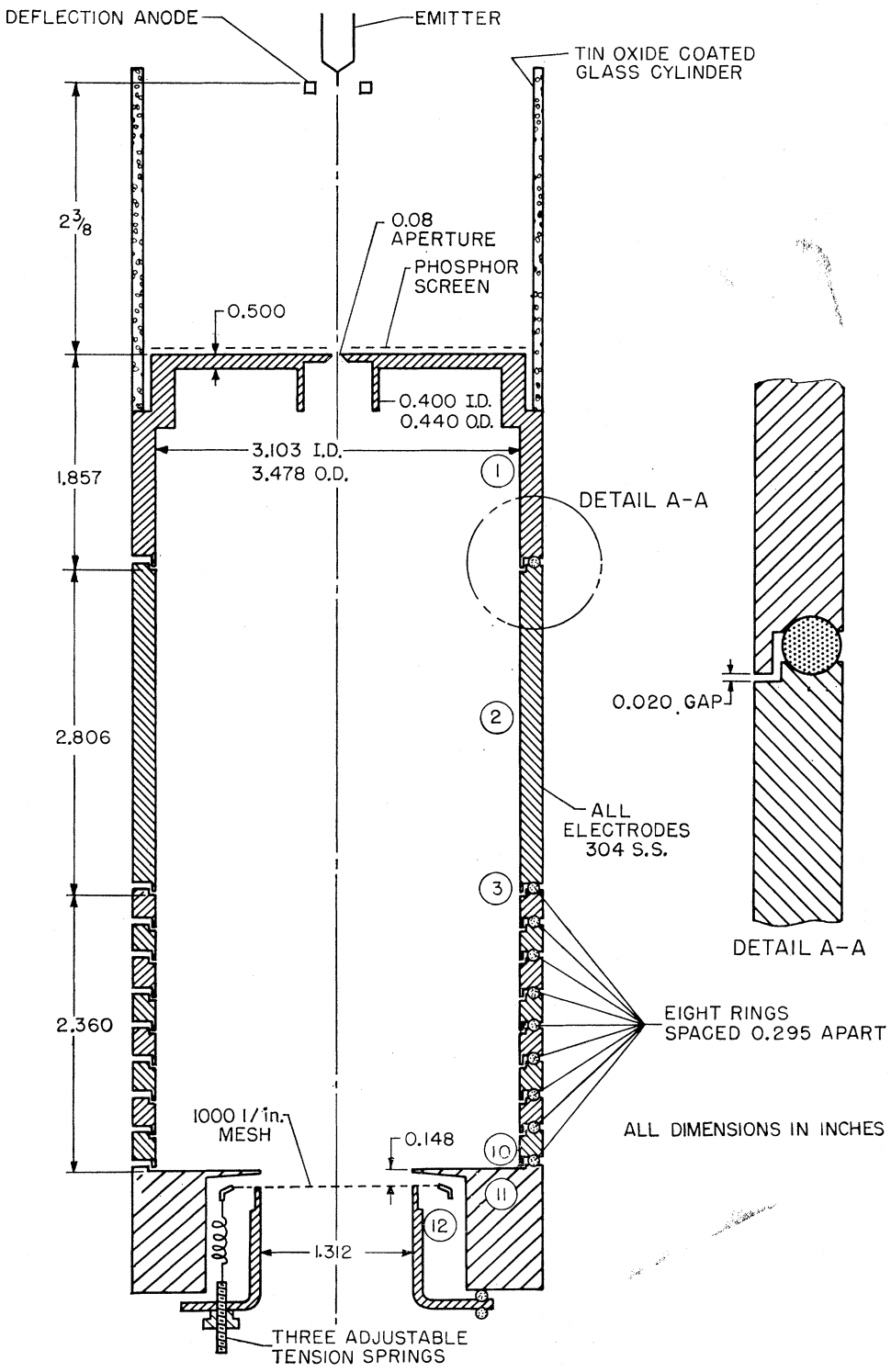


FIG. 5. Dimensioned diagram of high-resolution version of field-emission energy analyzer. Stainless-steel electrodes are cylindrically symmetric except for sapphire-ball mounting system. Electrode dimensions were held within 1 mil by alternate machining and annealing at 700°C. All electrode edges were provided with at least a 10-mil radius.

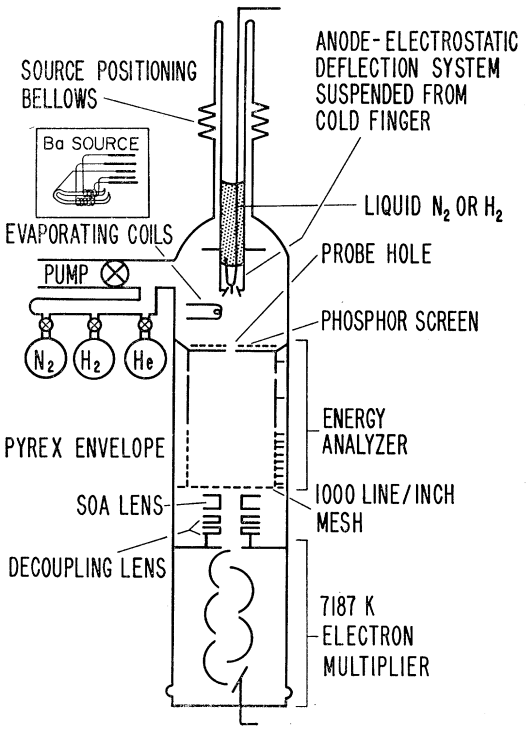


FIG. 6. Schematic drawing of the field-emission retarding energy analyzer used in this study. An enlarged view of the Ba source is shown in the top right-hand side.

## III. EXPERIMENTAL

### A. Field-Emission Energy Analyzer

The retarding-potential energy analyzer used in this study is a one-third-scale version of a higher-resolution instrument which has been briefly described.[35,36] The previously used spherical retarding-potential analyzer[37] had three serious limitations: (1) secondary electron emission from the retarding element, (2) poor sensitivity, and (3) long time constant. While these limitations could have been removed by employing a spherical retarding mesh followed by an electron multiplier, it was not deemed practical to construct a bakeable spherical mesh of sufficient precision to meet the resolution requirements. Instead, the radially diverging electron beam from the emitter was focused beneath the imagining screen to form a parallel beam. This beam was retarded by a series of cylindrical rings and a 1000-line/in. flat mesh followed by an electron multiplier. The arrangement of the electrodes is shown in Fig. 5.

An analog computer was used to carry out the electron optical design which was subject to the following design constraints: (1) resolution for 2000-eV electrons to be about 10 meV, (2) 8-cm field-emission fluorescent screen provided with a 0.080 in. electron-beam probe hole in the center, (3) probe hole to be the aperture stop of the electron optical system and to be kept essentially field free, (4) sizes and shapes of electrodes as well as mesh hole size to be determined by resolution requirements, and (5) construction to be compatible with $10^{-13}$ Torr vacuum conditions after 400°C bake. A shielding cylinder was provided just below the anode probe hole to reduce the probe-hole field to a negligible value. The mesh surface was coated with a few hundred Angstroms of platinum black to assure a unipotential surface. The mesh was kept flat within 1 mil over its entire surface. Magnetic fields were minimized by careful shielding.

The inherent resolution of the instrument is determined by three factors: (1) product of the field at the mesh surface and the mesh hole size, (2) aberrations in the electron optical lenses, and (3) failure of actual electrodes to conform in dimensions and alignment to the computed electrode configuration.

The first resolution-limiting factor can be evaluated by estimating the potential difference between the center of a mesh hole and the edge since this approximates the full energy spread of the mesh transmission function. Glaser and Henneberg[38] has shown that the potential difference $\Delta V$ between the axis and the edge of a circular aperture is approximately

$$\Delta V = 2\pi^{-1}R(E_2 - E_1), \qquad (1)$$

where $E_2$ and $E_1$ are the electric field strengths above and below the aperture. Since the mesh used in the present instruments has an optical transparency of less than 50%, each mesh hole will be considered as an isolated circular aperture of radius $0.62\times10^{-3}$ cm (0.25 mil). The analog computer calculation for the case of a 2000-V field emitter predicted a 20-V/cm field above the mesh. The field below the mesh will be at least an order of magnitude less than this, yielding a value for $e\Delta V \sim 8$ meV. The contributions of the field and mesh size to the FWHM of the transmission function is thus less than 8 meV.

The second resolution-limiting factor was minimized by the field-free aperture stop and the very small beam diameter relative to the electrode diameters. The only appreciable contribution, due to spherical aberration of the first lens consisting of elements (1) and (2), (Fig. 5) is estimated to be less than $10^{-4}$ meV.[39] The third resolution-limiting factor, electrode shape, and alignment factors required a diameter and alignment tolerance of 0.1% for the analyzer electrodes in order to limit the contribution of this factor to 1 meV.[39] To achieve this end, machining tolerances were conservatively set at 1 mil. The estimated over-all resolution of

[35] R. D. Young and H. E. Clark, Proceedings of the Twelfth Field-Emission Symposium, 1965 (unpublished).
[36] For a general discussion of retarding energy analyzers see J. A. Simpson, Rev. Sci. Instr. **32**, 1283 (1961).
[37] R. D. Young and E. W. Müller, Phys. Rev. **113**, 115 (1959).
[38] A. Glaser and W. Henneberg, Zh. Techn. Fiz. **17**, 222 (1935).
[39] V. K. Zworykin, G. A. Morton, E. G. Ramberg, J. Hillier, and A. W. Vance, *Electron Optics and the Electron Microscope* (John Wiley & Sons, Inc., New York, 1945).

the high-resolution instrument was thus less than 10-meV FWHM. It is theoretically possible to improve the analyzer resolution considerably by decreasing the potential on electrode number 1. While this would increase the field-emission image size, it would decrease all the potentials on electrodes down to the retarding mesh, thus improving the inherent analyzer resolution.

Details of the analyzer construction are shown in Fig. 5. The cylindrical electrodes were stacked in a column and were electrically insulated from each other by three precise $\frac{1}{8}$-in. sapphire balls. The electrode column was aligned within 1 mil in all diamensions and clamped with long rods and springs in line with each column of sapphire balls. Pumping ports were provided at each ball socket and at all other "blind" volumes in the system. The electrodes were arranged to overlap so that potentials outside the electrodes could not influence the electron beam. The retarding mesh consisted of a 50% transparency, 1-mil-thick nickel mesh stretched tightly over a cylinder and maintained flat within 1 mil over its entire surface.

The instrument used in the present experiments (Fig. 6) is a one-third-scale version of the high-resolution instrument except that it also employs a 1000-line/in. mesh. Since resolution scales for fixed mesh sizes, it has a nominal resolution of 30 meV, which agrees with best measured resolution.[40] The combined anode-electrostatic deflection system is arranged so that any crystallographic plane can be positioned over the probe hole. A properly balanced voltage divider supplies symmetric voltages to the two pairs of deflection plates so that FN measurements for a particular plane can be made without repositioning the pattern. A Soa[36] lens together with two decoupling lenses focus the transmitted electrons onto the first dynode of an electron multiplier in such a way that the area of electron impact on the dynode is independent of the mesh potential. The emitter must be positioned within a few mils of the electron optical axis of the instrument for best resolution. This is achieved by suspending the cold finger from a bellows-gimbal assembly equipped with fine positioning screws. The electrical leads to the emitter are brought out above the bellows through the side of the glass cold finger so that a cryotip refrigerator may be inserted into the cold finger to provide liquid-hydrogen cooling.

A block diagram of the electrical system is shown in Fig. 7, along with all of the relevant potentials. The ratio of the potential $V_2$ with respect to the anode potential $V_1$ was found to be very critical. When the tip was positioned properly on the optical axis of the system the ratio of $V_2$ to $V_1$ was 0.11 (depending slightly upon the tip-to-screen distance). This ratio always decreased if the system was not aligned properly. The tip was held at ground potential while the potential of the mesh was swept. All of the potentials immediately above and below the mesh were fixed with respect to the mesh potential (Fig. 7) as it changed. The anode and lower decoupling lens potentials are with respect to ground. Also the potential of the first dynode of the multiplier is held at a fixed voltage independent of the applied voltage on the multiplier.

In a retarding-potential energy analyzer the emitted electrons with total energy $E$ will pass through the mesh if

$$E > \varphi_m + E_F - V_m, \tag{2}$$

where $\varphi_m$ and $V_m$ are the work function and applied potential of the mesh, respectively, and $E_F$ is the Fermi energy. Thus the total energy distribution is the differential with respect to energy of the measured current $j(E)$:

$$j(E) = \int_E^\infty j'(E)\, dE, \tag{3}$$

where $j'(E)$ is the total energy distribution.[32] The signal from the analyzer is differentiated electronically by using a lock-in amplifier. The tip was modulated with respect to ground with an ac signal of 10-mV peak-to-peak (P-P) amplitude at the reference frequency. This frequency component of the output signal was recorded, giving the energy distribution $j'(E)$ directly.

The system was pumped by two mercury diffusion pumps in series. The nominal background pressure, as measured by a Redhead gauge, after thorough outgassing and 400°C bakeouts was $\sim 10^{-12}$ Torr.

### B. Sources of Ca, Sr, and Ba

The Ca and Sr sources were prepared by coating a small coil of 5-mil Mo wire supported on 0.010-mil tungsten outgassing loops with either $CaCO_3$ or $SrCO_3$. The spectroscopically pure carbonate was suspended in an acetone solution and sprayed onto the Mo filament. These sources were then activated inside the vacuum system by heating to approximately 1250°K for Ca and 1100°K for Sr.[41] The sources would then produce atoms of either Ca or Sr when heated to approximately 1450 or 1200°K, respectively. The sources had to be replaced if the system was opened after they had been activated.

The Ba source was prepared from commercially produced 6-mm nickel or iron tubing containing distilled Ba. A piece of the tubing approximately 2 in. long was bent into a hairpin shape (see insert of Fig. 6), with both ends crimped closed. This hairpin was supported in spring tension by two 12-mil tungsten outgassing loops with small coils at the ends to accept the tubing. The tubing was outgassed in an auxiliary vacuum system at $\sim$1400°K for at least 24 h. After this initial outgassing it was sealed into the vacuum system and outgassed again. When the source was ready to be opened a capacitor was discharged between the tubing and a

[40] R. D. Young and C. E. Kuyatt, Rev. Sci. Instr. **39**, 1477 (1968).

[41] G. E. Moore and H. W. Allison, J. Chem. Phys. **23**, 1609 (1955).

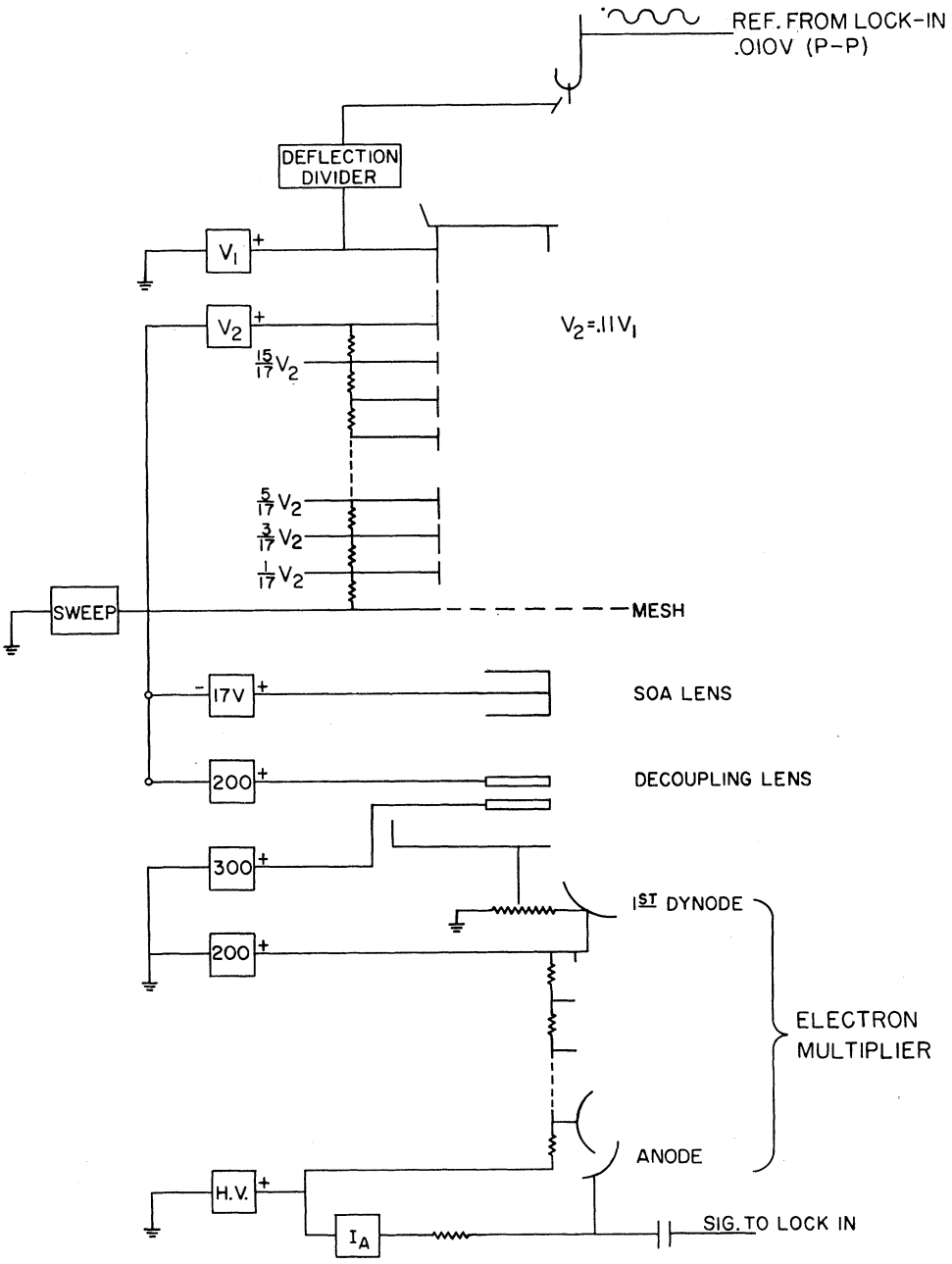


FIG. 7. Block diagram of the electrical system, including relevant potentials.

small tungsten wire positioned at the point to be opened (see insert in Fig. 6). This technique proved to be very satisfactory. The pressure would remain in the $10^{-11}$-Torr range or low $10^{-10}$ Torr when the Ba source was heated to produce Ba. After the Ba was thermally desorbed no traces of contaminant gases were seen in the field-emission pattern.

### C. Procedure and Data

The tungsten field emitter was flashed clean and then annealed. The crystallographic plane to be studied was positioned over the probe hole by adjusting the voltage on the deflection plates, while maintaining the image of the tip on the optical axis by using the bellows and gimbal arrangement. Then an energy distribution for the clean surface was taken. The sensitivity of the instrument was such that a usable energy distribution could be obtained for a total current through the probe hole in the $10^{-13}$ A range, for a reference frequency of 250 Hz at a 10-mV (P-P) amplitude and a 2-sec time constant for the lock-in amplifier. After the total energy distribution for the clean surface was recorded the

total current through the probe hole was monitored as the source was heated. The arrival of a single atom could be easily detected as a sharp rise in the total current. The noise in the energy distribution after the adsorption of one atom was always greater than the equivalent noise in the clean energy distribution.[10,27] Consequently, the bulk of this work was conducted at 78°K; but in the case of Sr the noise was too great at 78°K and the temperature was lowered to 21°K. Presumably this flicker noise is directly related to the diffusion process of the adsorbate. In fact at temperatures much above 78°K the adsorbates actually move out of the view of the probe hole (especially Sr). At room temperature all these adsorbates are mobile. The temperature dependence of the amplitude of the flicker noise probably is directly related to the diffusion energy.

The energy distribution after adsorption was divided by the clean energy distribution to obtain an experimental enhancement factor $\mathfrak{R}(E)$. $\mathfrak{R}(E)$ is not the total enhancement factor $R(E)$ which we need to relate to the theory for two reasons: (1) We have sampled an area of the surface large compared to the effective area of the adsorbate; and (2) the energy distribution can be affected by the macroscopic properties of the adsorbate-surface interaction, such as work function change, field enhancement, or polarization. If we sample with the probe hole a surface area $A_0$ with an energy distribution $j_0'(E)$ per unit area, and the adsorbate potential well has an effective area $A_a$ which yields an energy distribution through this area, per unit area, $j_1'(E)$, then we can write $\mathfrak{R}(E)$ as

$$\mathfrak{R}(E)=\frac{A_a j_1'(E)+(A_0-A_a)j_{0'}'(E)}{A_0 j_0'(E)}, \tag{4}$$

where we have lumped all changes in the energy distribution caused by macroscopic properties of the adsorbate-substrate interaction into $j_{0'}'(E)$. The total enhancement factor $R(E)$ is defined as

$$j_1'(E)\equiv R(E)j_0'(E). \tag{5}$$

In general, $A_0 \gg A_a$ and $j_{0'}'/j_0' \sim 1$ so we can reduce Eq. (4) using (5) to

$$\mathfrak{R}(E)=\frac{A_a}{A_0}R(E)+\frac{j_{0'}'(E)}{j_0'(E)}. \tag{6}$$

The last term in Eq. (6), which results from the macroscopic properties of the system will not be exactly unity, but its energy dependency will be small. It is easy to show that long-range potentials such as dipole moments cannot affect the energy dependence nearly as drastically as the quantum-mechanical effects which are included in the enhancement factor $R(E)$. We will subsequently show that the possible effects contained in $j_{0'}'/j_0'$ are grossly inadequate to explain the observed experimental enhancement factors $\mathfrak{R}(E)$. Consequently, $j_{0'}'/j_0'$ was usually taken to be a constant in analyzing the data.

We have implicitly assumed in Eq. (6) that the emission from the clean surface results from a nearly free-electron gas: That is all the electrons which are tunneling from within the metal have the same properties, i.e., a parabolic band. If we had contributions from a narrow $d$ band and a broad $s$ band in our original distribution we could obtain structure in the $\mathfrak{R}(E)$ curve which did not reflect directly the properties of the energy levels of the adsorbate atom but instead the characteristics of the tunneling process for different types of electrons.[34] For example, if structure in the $\mathfrak{R}(E)$ factor appeared in the same crystallographic direction for different adsorbates it must be considered very suspect. In a later section we will use the energy distribution from the (100) plane of tungsten[27,33] to demonstrate the effect of band structure on the enhancement curves.

In Fig. 8, we show the experimental energy distribution from the (111) and (112) planes of a tungsten crystal at 78°K. The theoretical curves are calculations of the total energy distribution from a free-electron metal,[32] where

$$\begin{aligned} j'(E)&=J_0 e^{\epsilon/d}/d(1+e^{\epsilon/kT}),\\ \epsilon&=E-E_F,\\ J_0&=\frac{e^3F^2}{8\pi h\varphi t^2(y)}\exp\left(\frac{-4(2m\varphi^3)^{1/2}v(y)}{3heF}\right),\\ d&=heF/2(2m\varphi)^{1/2}t(y), \end{aligned} \tag{7}$$

where $E_F$ is the Fermi energy, $F$ is the applied field in V/cm, $J_0$ is the current density in A/cm² at $T=0$°K, $m$ and $e$ are the mass and charge of the electron, $\varphi$ is the work function of the metal, and $t(y)$ and $v(y)$ are the image-correction terms,[42] which are slowly varying functions of $y=(e^3F)^{1/2}/\varphi$. The form of the energy distribution from the (111) plane is exactly what one expects from a free-electron metal. The deviation at lower energies between the experimental and theoretical curve results from the approximation used in calculating the tunneling probability. It is usually calculated in a WKB approximation,[42] expanding about $E_F$, and neglecting quadratic and higher-order terms. If the quadratic term is maintained, the theoretical curve would coincide with the experimental curve, over this energy range. The (111) plane of tungsten should be an ideal test for the FN theory. There are no expected band-structure effects[43] and the metal should behave like a nearly free-electron metal over the energy range that is measured. But the work function we calculated

[42] R. H. Good and E. W. Müller, *Handbuch der Physik* (Springer-Verlag, Berlin, 1956), Vol. 21.

[43] L. F. Mattheiss, Phys. Rev. **139**, 1893 (1965); T. L. Loucks, *ibid.* **143**, 506 (1966).

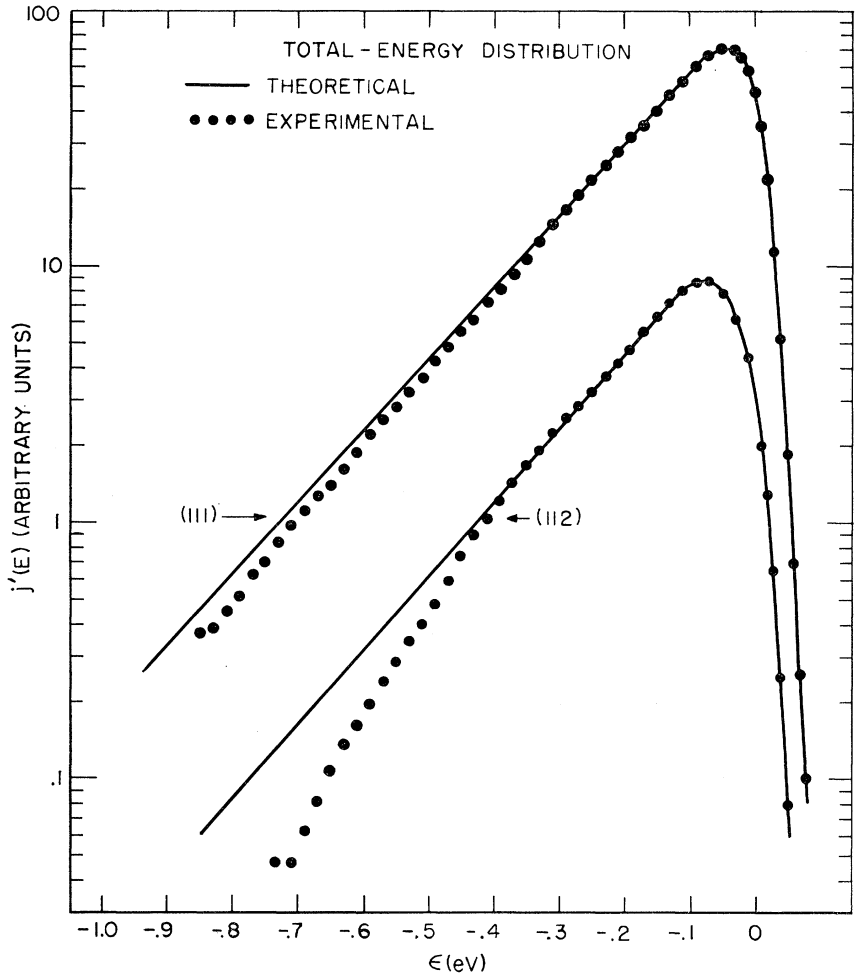


FIG. 8. Measured total energy distribution $j'(E)$ for the (111) and (112) planes of tungsten ($\epsilon=E-E_F$). The theoretical curve is the first-order expansion of the WKB tunneling probability (Ref. 42). The deviation at low energies of the (112) plane energy distribution is unexplainable in the FN theory.

from combining the slope of the FN plot and the energy distribution[26] is approximately 4.8 eV. While this is in excellent agreement with measurements of the same type by Swanson and Crouser,[27] it is much higher than values obtained using other techniques. The detailed shape of the energy distribution is much more sensitive to the actual shape of the surface potential and band structure than is the slope of the FN. Therefore, the energy distribution must be used with caution in measuring work functions.

The deviation of the (112) plane energy distribution is more severe and cannot be explained in terms of the FN model. The drop in the energy distribution at lower energies is too dramatic to be due to the higher-order terms in the tunneling probability. This could be a band-structure effect or an impurity on the (112) plane which is not removed by high-temperature flashing. In either case it could give anomalous enhancement-factor curves for adsorption on the (112) plane. We will point this out again when we introduce the enhancement curves for the (112) plane.

To illustrate the effect that the substrate can have on the enhancement factor curves we studied Ca adsorbed on the (100) plane of tungsten. The energy distribution from this plane, first observed by Swanson and Crouser,[27,33] contains an additional peak approximately 0.4 eV below the Fermi surface. Curve No. 1 of Fig. 9 is the energy distribution from the thermally flashed and annealed (100) tungsten plane. The curve marked 0 is the FN ideal energy distribution, to which the actual energy distribution No. 1 converges at both ends. Energy distribution No. 2 is after deposition of one Ca atom. It is obvious from the relative changes between No. 1 and No. 2 that the Ca atom has little influence on the energy distribution near the hump. In Fig. 10, we have calculated the enhancement factors corresponding to the energy distributions shown in Fig. 9. $j_1'/j_0'$ is the differential current-density ratio for the actual (100) plane energy distribution with respect to the ideal free-electron energy distribution. This bell-shaped "enhancement factor" did not shift its peak position or change its shape as the field and temperature were varied, indicating that it truly originates from within the metal surface. $j_2'/j_1'$ is the enhancement factor for the Ca atom on the (100) plane. It is apparent that the minimum in the enhancement

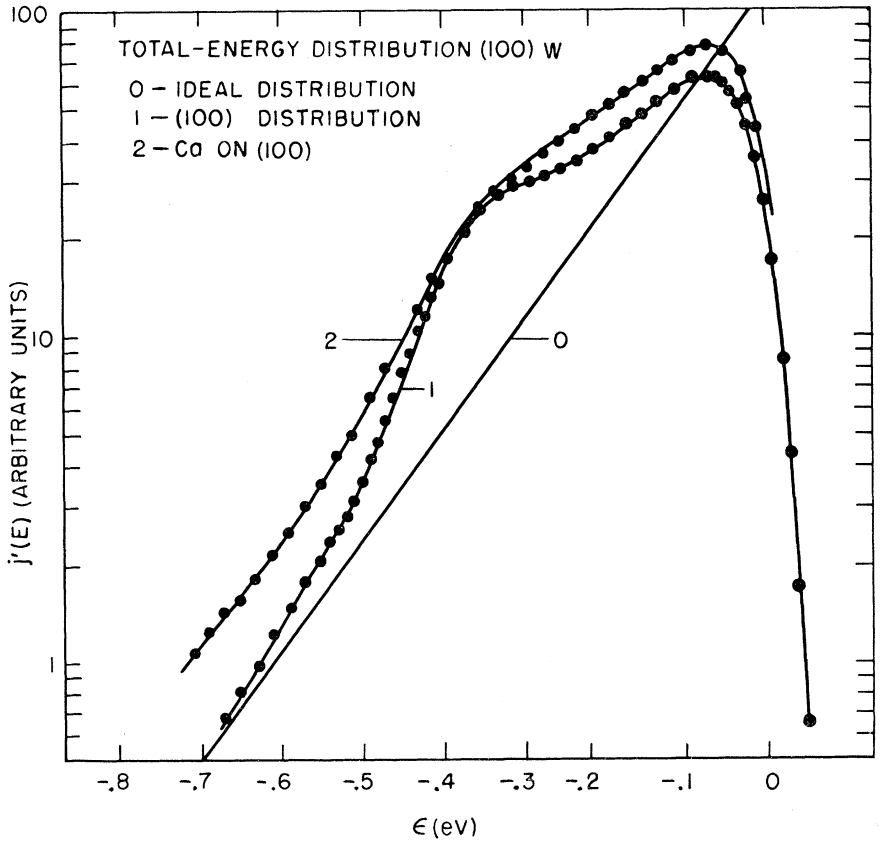


FIG. 9. Total energy distribution from the (100) plane of $W$, (1) before, and (2) after the deposition of one Ca atom, the curve labeled 0 is the ideal FN total energy distribution where $\epsilon = E - E_F$.

curve is due to the presence of the additional peak in the original energy distribution. This enhancement factor goes to unity at the peak in the hump, telling us that the Ca atom has little effect on these electrons. Therefore, the enhancement-factor curve reflects the properties of the electrons tunneling from the metal not the electronic properties of the adsorbate. It was observed that if the current from the hump $[j_1'/j_0']$ was divided out of energy distribution No. 2 and the enhancement factor calculated from the ideal energy

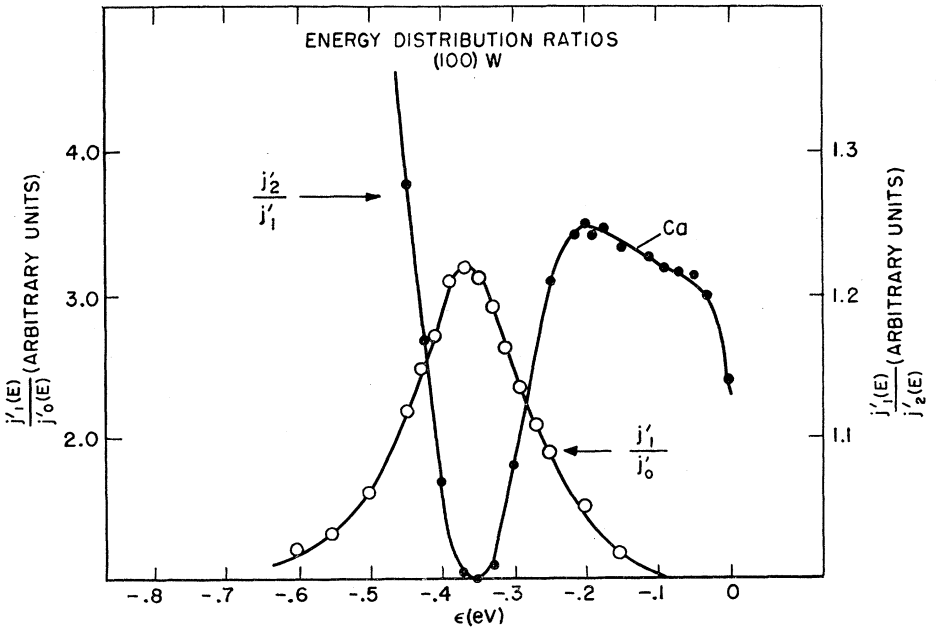


FIG. 10. Enhancement factors calculated from Fig. 9. $j_1'/j_0'$ is for the measured (100) plane energy distribution relative to the ideal FN energy distribution ($\epsilon = E - E_F$). $j_2'/j_1'$ is for one Ca atom on the (100) plane, relative to the measured energy distribution. The decrease in $j_2'/j_1'$ is caused by the increase in $j_1'/j_0'$.

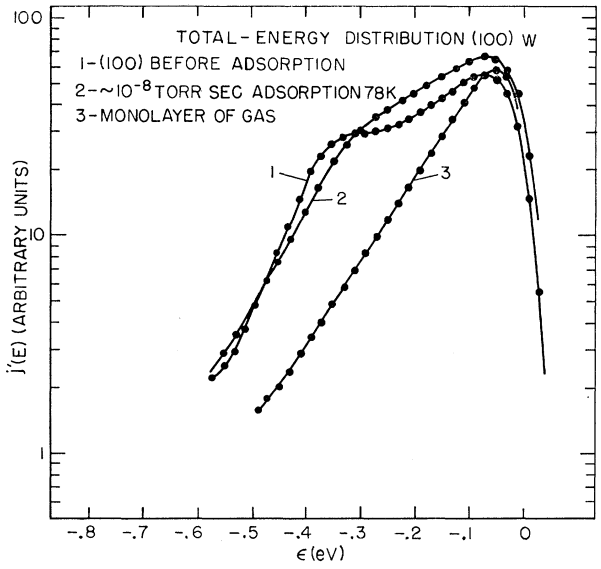


FIG. 11. Effect of contamination (probably CO) on the (100) tungsten plane energy distribution ($\epsilon=E-E_F$). Curve No. 1 is before any adsorption had taken place; No. 2 is after approximately $10^{-8}$ Torr sec adsorption at 78°K; and No. 3 is after the tip had warmed up to room temperature. All three curves are on the same scale, while the ratios of total currents were $I_2/I_1=1.1$, $I_3/I_1=0.63$.

distribution $j_0'(E)$, an enhancement factor for Ca was obtained which agreed qualitatively with the factors obtained on the (013) plane. Finally, even though the total current increased upon adsorption of Ca the change in the slope of the FN curve does not yield an accurate work-function change. This is probably the reason that the work-function–versus–coverage curves of Schmidt and Gomer[44] for K and Schmidt[45] for Ba have unusual behavior at low coverages, on the (100) plane.

We digress for a paragraph to report and speculate about some curious observations of the effect of contamination (probably CO) on the hump on the (100) plane. In Fig. 11, energy distribution No. 1 is before any adsorption, No. 2 is after $10^{-8}$ Torr sec exposure to the residual gas at 78°K and No. 3 is after the tip had warmed up to room temperature and had remained there overnight. All three curves are reproduced on the same scale, indicating that the major effect of this contaminant is to eliminate the hump. If the hump originates from a tight-binding $d$-like band as Gadzuk has postulated,[34] we can speculate that the covalent bonding of the contaminant gas changes the character of the atomic $d$ orbitals of the surface tungsten atoms which bond to it. Therefore, by removing or changing the nature of the atomic $d$ orbital of the surface atom, tunneling from the $d$ band must originate from the second layer in this tight-binding picture, effectively increasing the tunneling barrier or reducing the current.[34] In contrast, the alkali or alkaline-earth adsorbates do not basically bond covalently and consequently do not remove the hump caused by the $d$ band.

The enhancement factors for single Ba, Sr, and Ca atoms were measured on the (110), (112), (111), and (013) planes of tungsten. The (013) plane was substituted for the (100) plane since we are unable to analyze the data on that plane. Figure 12 contains a series of runs taken for a single Ba atom on the (111) plane of tungsten at 78°K. Each run represents a new Ba atom deposited after the tip was flashed clean and annealed. The lower three curves are cases where gas atoms were adsorbed before the Ba atom arrived. The arrival of a contaminant which decreased the current was as noticeable as the arrival of the electropositive adsorbate. The variation in the upper curves is inherent in the system. For the same Ba atom each curve could be reproduced but for every new adatom, a slightly different curve would result. This sensitivity to the exact placement of the adsorbate atom is consistent with the theory of tunneling resonance presented in the following paper. Gadzuk[23] found that the exact magnitude of the enhancement factor was extremely sensitive to the adsorbate-substrate parameters, whereas the peak positions are relatively insensitive. The shift of the sharp peaks in Fig. 12 is induced by changing the field. The shift in the peak position with field for Ba on the (111) tungsten plane was $\Delta E/e\Delta F=1.3\pm0.3$ Å (Fig. 12).

Since the enhancement curves are obtained by dividing two exponential curves into each other, the structure in any one curve would be quite suspect. But these curves are reproducible; we have made over 100 runs for Ba on about six different faces of tungsten and of those runs only about 10% did not exhibit the same basic structure on any given plane.

In Fig. 13, we have again reproduced a typical enhancement factor for a Ba atom on the (111) plane of tungsten, in order to illustrate the deviation of these curves from changes expected from FN theory. Curves No. 1 and No. 2 are calculated from Eqs. (5) and (7) assuming that the total measured current increase resulted from a work-function change or from a field enhancement, respectively. Neither curve comes close to explaning the dramatic energy dependence of the experimental enhancement factor. Curves 1 and 2 are upper limits to these effects since the change in the slope of the FN curve indicated a smaller resultant change in the work function than the total current increase did. In other words the preexponential has increased without a corresponding decrease in the work function (a characteristic of tunneling resonance). If the enhancement curve for a work-function change is calculated from the change in the slope of the FN curve, it would be nearly a horizontal line on Fig. 13 at $\mathfrak{R}(E)\sim1$–1.2. Thus we have taken $j_0'/j_0'$ in Eq. (6)

[44] L. D. Schmidt and R. Gomer, J. Chem. Phys. **45**, 1605 (1966).
[45] L. D. Schmidt, J. Chem. Phys. **46**, 3830 (1967).

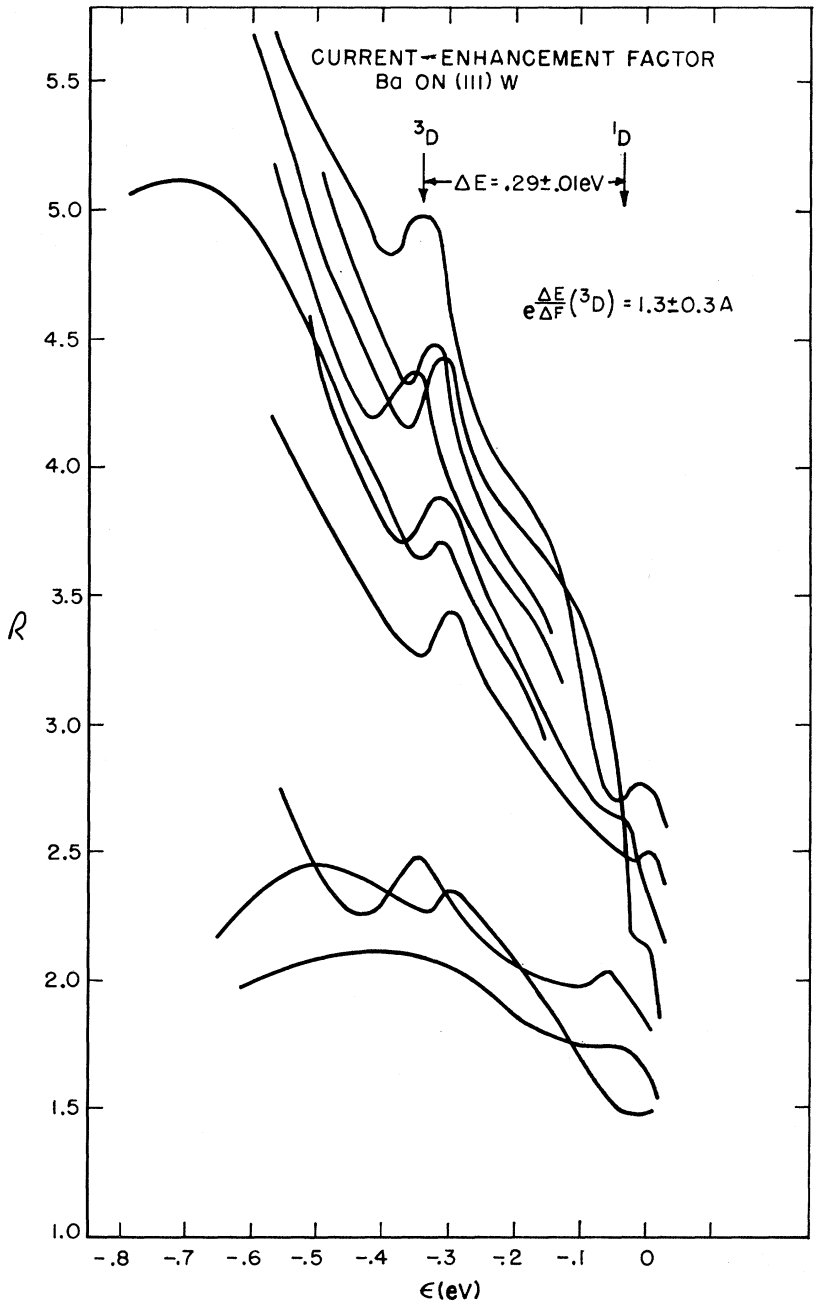


FIG. 12. Experimental enhancement factor for single Ba atoms on the (111) plane of tungsten. The three lower curves represent cases where adsorption of electronegative gases was observed before the Ba atom arrived. The shift in the narrow peaks with field was $\Delta E/e\Delta F = 1.3 \pm 0.3$ Å, while the peak separation was $0.29 \pm 0.01$ eV where $\epsilon = E - E_F$.

to be unity and Eq. (6) becomes

$$R(E) = (A_0/A_a)[\mathfrak{R}(E) - 1]. \tag{8}$$

The ratios of the effective areas $A_0/A_a$ can not be determined very accurately. In principle, we could calculate $A_0$ from the measured current using the FN theory;[31] but the ability of the FN theory to predict the actual current density from individual crystal planes has never been adequately checked. Also, the effective area of the adsorbate potential $A_a$ is just as obscure. It is fortunate that at this stage of the development of tunneling resonance we do not need a reliable determination of $A_0/A_a$ because the essential physics is contained in the shape and position of the structure in the experimental enhancement factor. When we have an accurate model for the three-dimensional tunneling through an adsorbate, the actual value of $A_0/A_a$ will be needed to verify the theory. To obtain an approximate value of $A_0/A_a$, the radius of the tip was estimated from the total-current characteristics[46] and the fraction of the surface sampled by the probe hole calculated.

[46] See Gomer, Ref. 18, p. 47.

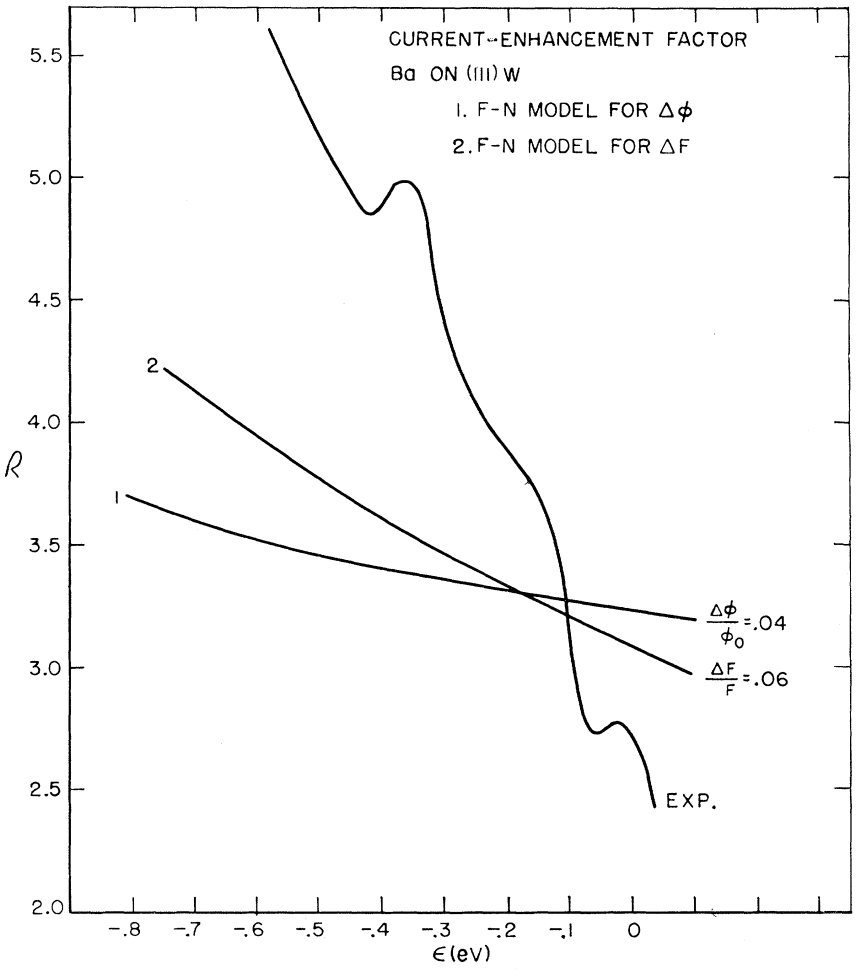


FIG. 13. Comparison of the experimental enhancement factor for Ba on the (111) plane and the calculated changes from FN theory. Curves No. 1 and No. 2 are calculated from the FN equation assuming that the change in total current upon adsorption resulted from a work function $\Delta\varphi$ or field change $\Delta F$, respectively, where ($\epsilon = E - E_F$).

$A_a$ was taken as 1 Å$^2$ in all cases yielding $A_0/A_a$ approximately $10^3$–$10^4$.

Figures 14–17 show the experimental enhancement factors for Ba and Ca on the (110), (112), (111), and (013) planes of tungsten and Sr on the (110) and (111) planes. We will discuss each adsorbate separately in the following sections, showing the relationship between the observed structure in the enhancement factors and the energy levels of the broadened and shifted atomic levels of the isolated atom.

### 1. *Ba on Tungsten*

An isolated Ba atom has a $6s^2$ ground-state configuration above the closed shell of the xenon atom. This state is at −5.2 eV relative to the vacuum level while the first and second excited states of Ba are a triplet $^3D$ $6s5d$ state between −4.02 and −4.09 eV and a singlet $^1D$ $6s5d$ state at −3.80 eV.[47] When the atom interacts with the surface of the metal the $6s^2$ ground state will be broadened and shifted.[14–16] This broadened and shifted $6s^2$ virtual level may overlap the $6s5d$ excited levels which, because of the contracted nature of the $5d$ electron relative to the $6s$, will not be shifted or broadened as much. A schematic picture of the broadening and shifting of the levels as the Ba atom is brought up to the surface is shown in the left-hand side of Fig. 18. If the excited $d$ levels lie below the Fermi surface, the ground-state configuration of a Ba atom on a tungsten surface could be a mixture of $s$- and $d$-type states. The structure appearing in the enhancement-factor curves for Ba (Figs. 14–17) has exactly these characteristics. On the low work function (013) and (111) faces three peaks are observed: a broad level lower in energy which originated from the ground-state $6s^2$ level and two sharp levels at higher energies which can be related to the triplet $^3D$ and singlet $^1D$ $6s5d$ excited states of Ba. The separation in energy between the peaks identified as the triplet state $^3D$ and the singlet state $^1D$ was observed to be 0.29±0.01 eV on all low work-function planes where both peaks were simultaneously seen (Fig. 12). This is exactly the separation between the two $m=0$ states of the singlet

[47] Charlotte E. Moore, *Atomic Energy Levels*, Natl. Bur. Std. Vols. I–III (U. S.) Circ. No. 467 (U. S. Government Printing Office, Washington, D. C., 1958).

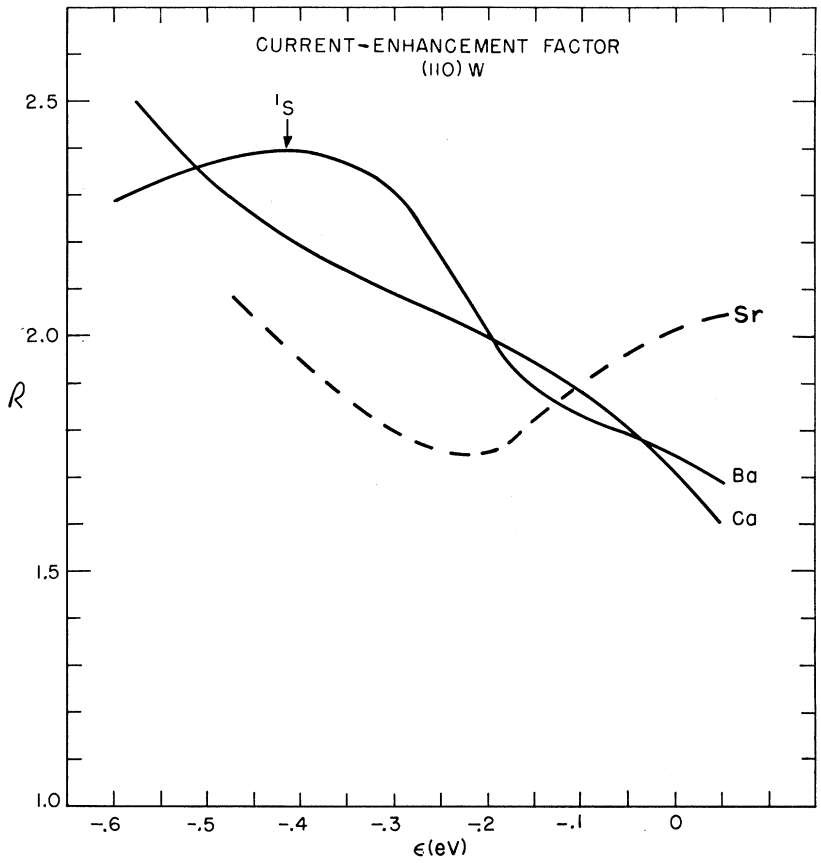


FIG. 14. Experimental enhancement factor $\mathcal{R}$ for Ba, Sr, and Ca on the (110) plane of tungsten, where $\epsilon=E-E_F$.

and triplet states in the isolated atom.[48] Gadzuk[49] has shown quite generally that the relative shift of the singlet with respect to the triplet $6s5d$ state should be zero, and has suggested why the $m=0$ state should be the primary contributor to the resonance from the triplet state.

As we increase the work function $\varphi$ of the substrate $[\varphi(013)\leq\varphi(111)\leq\varphi(112)\leq\varphi(110)]$ the narrow $6s5d$ bands begin to disappear above the Fermi surface. On the (112) plane (Fig. 15) the singlet $^1D$ state is not visible and on the (110) plane (Fig. 14) both of the $6s5d$ levels are above the Fermi surface. The only visible state on the (110) plane is the broad $6s^2$ virtual level. A series of about twenty runs were made starting at the (013) plane and moving towards the (112) plane. In this region the work function measured by combining the FN slope with the slope of the energy distribution[26] seems to give reasonable values of from 4.35 eV on the (013) to ~4.7 eV near the (112) plane. When all these curves were corrected for the measured work function and the shift due to the field, which will be discussed later, the peak position of the triplet $^3D$ level coincided for all runs. On the other hand, when we reached the (112) plane the measured work function from this technique was approximately 5.3 eV, which was so large that even after field correction the position of the triplet $^3D$ level was far too low. This behavior was also found when the (110) region was sampled.[50] The position of a particular peak such as the triplet $^3D$ is determined by other factors than the work function of the substrate and the applied fields. It will depend, for example, upon the effective distance of the adsorbate from the surface, the net charge on the absorbate, and the screening distance at the surface.[14–17] Therefore, it should not be too surprising that changing the substrate has more of an effect on the atom-surface interaction than can be represented by a work-function change.

The general characteristics of the width and relative position of the three "atomic bands" for Ba can be determined from the enhancement-factor curves in Figs. 14–17, but to put their positions on an absolute energy scale we must know how the peaks shift with field and the work function of the substrate. To first order, the shift of the level with the field $F$ should be $qFs$,[16] where $q$ is the charge on the atom and $s$ is the effective atom-metal separation. In second order, the

[48] See Eq. (27) and Fig. 8 of the following paper (Ref. 23).
[49] See Eq. (25) of the following paper (Ref. 23).

[50] When the instrument was aligned properly on the (110) plane (which is difficult because of the exponentially rising current as you move away from the center of the plane), the work function obtained by combining the slope of the FN and energy distribution (Ref. 26) was $\varphi(110)\geq 5.7$ eV.

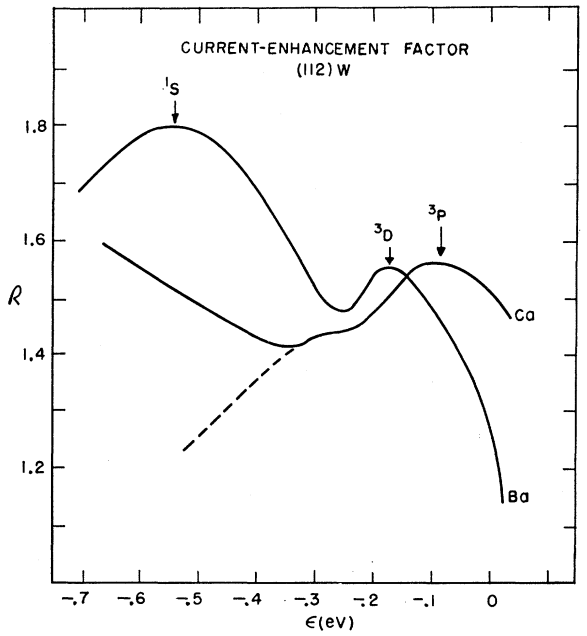


FIG. 15. Experimental enhancement factor $\mathfrak{R}$ for Ba and Ca on the (112) plane of tungsten ($\epsilon=E-E_F$). The dashed line for Ca is the proposed enhancement factor if the effects of the abnormal (112) energy distribution (Fig. 8) were removed.

position of the peak $E_\varphi$ depends upon the charge of the adsorbate which depends upon the field. In Bennett and Falicov's[16] self-consistent model the second-order change in $E_\varphi$ due to the change in the charge of the adsorbate resulted in approximately a 5% difference between the actual self-consistent field shift and the shift that would have been predicted from an $qFs$ shift for $K$ on tungsten.

The shift in the peak position of the $^3D$ peak with field measured on the low work-function (013) and (111) plane was $\Delta E_\varphi/e\Delta F^{(111)}=1.3\pm0.3$ Å and $\Delta E_\varphi/e\Delta F^{(112)}=1.7\pm0.8$ Å on the higher work-function (112) plane over about a 20% change in field. The scatter in the data was too large to determine if the field shift deviated from linearity. The field shift on the (110) plane could not be measured because the width of $6s^2$ level is too large compared with the expected field shifts, and the change in the nonresonant part of the tunneling with field can dominate the shift in a broad peak. The position of the triplet $^3D$ peak extrapolated to zero field on the low work-function (013) plane with $\varphi=4.35$ eV [27] is $4.20\pm0.1$ eV below the vacuum level. Therefore, within the error of our measurements and field extrapolation scheme there is no observable shift in either the triplet $^3D$ $6s5d$ or singlet $^1D$ $6s5d$ states of Ba when it interacts with the (013) plane [or the (111) plane, if $\varphi=4.4$ eV]. If the triplet $^3D$ state observed on the (112) plane is to be at the same position at zero field and our extrapolation scheme is correct, then $\varphi(112)=4.6\pm0.4$ eV.

To determine the peak position of the $6s^2$ level from the enhancement-factor curves we need the help of Gadzuk's theory,[23] since we have already seen in Fig. 2 that the peak in the enhancement-factor curve for a broad level does not occur at the peak in the level. Gadzuk's[23] calculation has reproduced the enhancement curves for Ba on the (013) and (111) planes where all three levels are seen simultaneously. In the zero-field limit his calculations show that the position of the virtual $6s^2$ ground state is at $E_\varphi{}^S=-4.25$ eV with a shift $\Delta E^S=0.95$ eV and a half-width $\Gamma_{6s}=0.75$ eV; the virtual $^3D$ $6s5d$ excited state is at $E_\varphi{}^{^3D}=-4.10$ eV with $\Delta E^{^3D}\approx0$ eV and $\Gamma_{^3D}=0.1$ eV; and the virtual $^1D$ $6s5d$ excited state is at $E_\varphi{}^{^1D}=-3.80$ eV with $\Delta E^{^1D}\approx0$ and $\Gamma_{^1D}=0.1$ eV. The peak corresponding to the $6s^2$ virtual level in the enhancement factor is shifted $\sim0.3$ eV below the actual position of the peak in the level due to the nonresonant contribution to the enhancement factor (Fig. 2).

For the purpose of interpreting resonance-tunneling data it would be extremely useful if Gadzuk's theory[23] were nothing more than a model where the above quantities were parameters which could be used to fit the data, but he has actually calculated all these quantities independently. The one exception to this statement is the observed zero shift $\Delta E^{^3D}\approx0$ of the triplet $6s5d$ state. This could result from the zero-field extrapolation scheme or the assumptions that had to be made to calculate $\Delta E^{^3D}$. Several of Gadzuk's calculations are so enlightening we shall make a brief comment on them here and refer the reader to the following paper for more details. The half-width of a single virtual level $\Gamma$ is proportional to the following matrix element:

$$\Gamma_i\propto|\langle m|V_m'|a_i\rangle|^2, \tag{9}$$

where $V_m'$ is the total potential outside the metal, with wave functions $\langle m|$, seen by the atomic electron with wave function $\langle a_i|$. The centrifugal barrier for the higher-angular-momentum $5d$ state results in a more localized wave function for the $5d$ state compared to the $6s$ state, consequently the matrix element in Eq. (9) is smaller for the higher-angular-momentum state. Gadzuk[23] used Slater functions for the two states to evaluate the ratio of the half-width and found that $\Gamma_D/\Gamma_S\approx0.1$ while $\Gamma_S$ had been calculated previously; $\Gamma_S\approx1$ eV.

The shift $\Delta E$ of an energy level as it interacts with the surface is proportional to[23]

$$\Delta E\propto\langle a_i|V_m'|a_i\rangle. \tag{10}$$

For the reason given above this matrix element will be smaller for the $6s5d$ levels than for the $6s^2$ level, which again is exactly what we observed. We should note that Gadzuk[23] found in performing his calculations that the relative peak heights were very sensitive to $\Gamma_S$ and $\Gamma_D$. For example, a 10% change in $\Gamma_D$ resulted in a significant change in the relative heights of the $^1S$

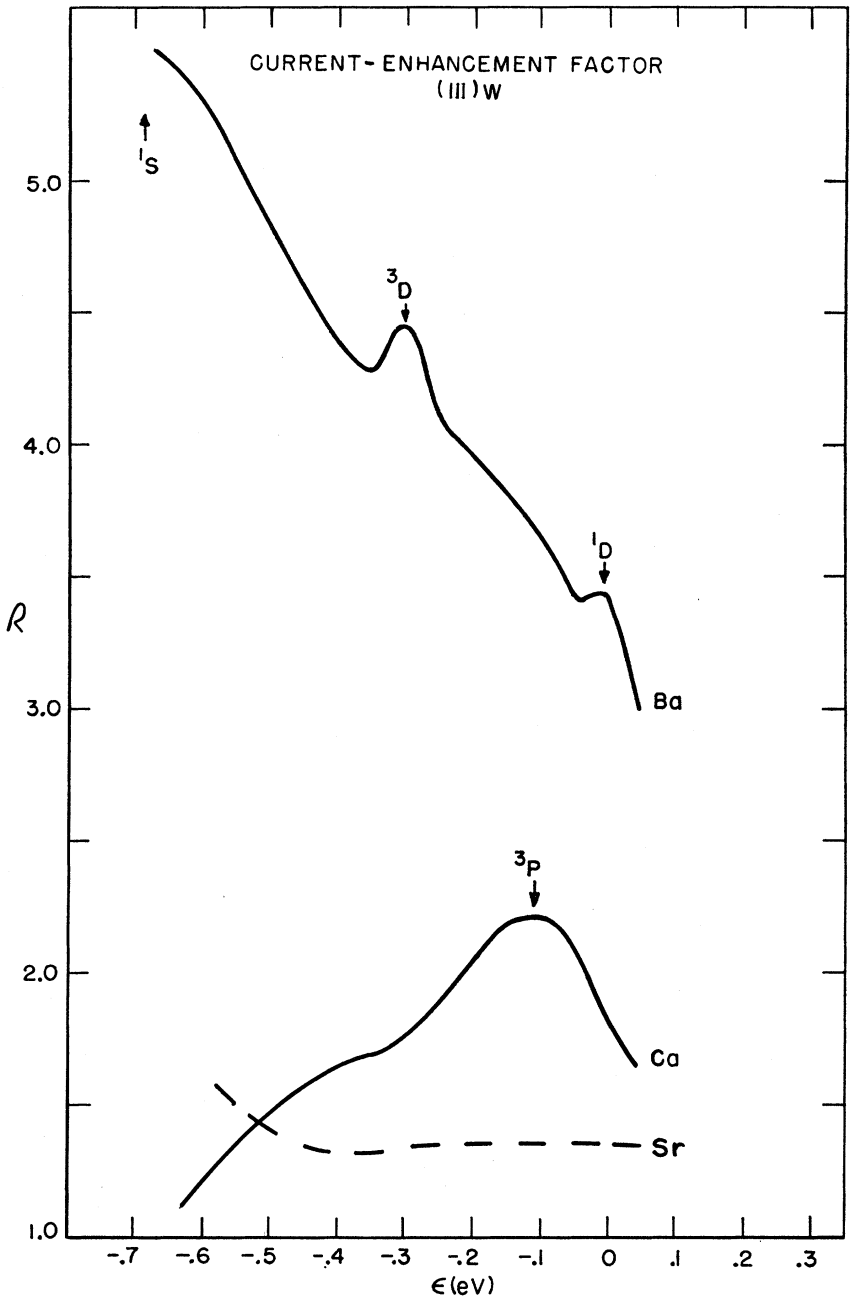


FIG. 16. Experimental enhancement factor $\mathcal{R}$ for Ba, Sr, and Ca on the (111) plane of tungsten, where $\epsilon = E - E_F$.

and $^3D$ peaks in the enhancement-factor curve. We have identified the structure in the enhancement-factor curves with the energy levels of the neutral Ba atom. When there are excited states visible below the Fermi surface we assume that there is a statistical weighing of the occupancy of the excited and ground states so that we are still observing an electropositive adsorbate. Presumably we could determine this statistical weighing factor from the relative amplitudes of the peaks if the theory was sufficiently detailed to treat this problem.

*2. Sr on Tungsten*

An isolated Sr atom has a $5s^2$ ground-state configuration which is 5.69 eV below the vacuum level. The first excited state is a triplet $^3P$ $5s5p$ at $-3.84$ to $-3.92$ eV.[47] The $5s^2$ ground-state level will be shifted upwards by about 1 eV when it interacts with the surface. The effect of the applied field and the nonresonant contribution to the tunneling will shift the peak in the enhancement factor down in energy by approximately 0.7 eV, so that we would expect to see a broad peak associated with the $5s^2$ level at approximately $-5.4$ eV. Therefore,

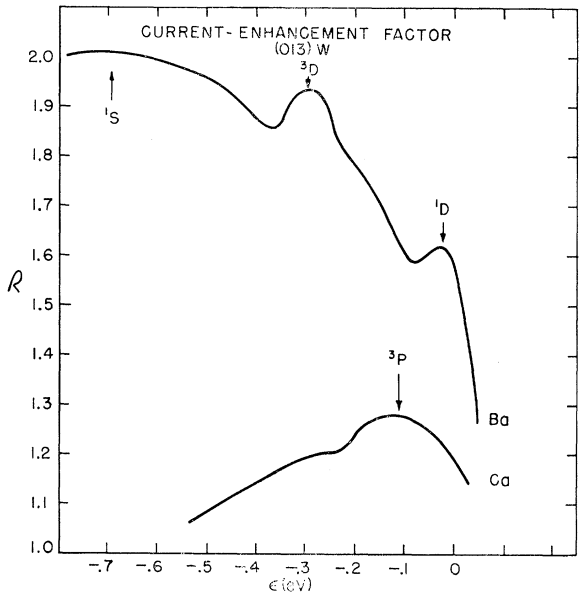


FIG. 17. Experimental enhancement factor $\mathcal{R}$ for Ba and Ca on the (013) plane of W, where $\epsilon=E-E_F$.

we would anticipate the effects of this virtual level only on the higher work-function planes. On the other hand, the first excited state, a triplet $^3P$ $5s5p$, will be shifted upwards and consequently out of view even on the low work-function planes.

Since we were never truly satisfied with the cleanliness of the Sr source we consider these data only preliminary, yet they seem to substantiate the above predictions. On the low-work (111) plane (Fig. 16) there is little sign of any energy levels for 0.6 eV below the Fermi surface. While on the high work-function (110) plane[50] the effects of a broad band near the Fermi surface is observed (Fig. 14). Here we can correlate our data with that of Clark and Young[10] for Sr on an oxygen-covered tungsten tip with a 6-eV work function. There they quite definitely saw the effects of a broad band above the Fermi surface (see Fig. 4): a dramatic increase in the logarithm of the slope of the energy distribution.

### 3. *Ca on Tungsten*

An isolated Ca atom has a $4s^2$ ground-state configuration 6.11 eV below the vacuum level, with its first excited state a triplet $^3P$ $4s4p$ at $-4.25$ eV.[47] If the ground state of Ca is shifted upon adsorption similar to Ba then the peak in the $4s^2$ level will lie too low to be observed. However, the $4s4p$ triplet state $^3P$ should be shifted upwards relative to the $6s5d$ Ba state and consequently be observable (see Fig. 18). Indeed Figs. 15–17 show the single $^3P$ level for Ca. On the higher function (110) plane the $^3P$ level is above the Fermi surface and is not visible. We believe the abnormal increase in the enhancement factor on the (112) plane (Fig. 15) at lower energies is a consequence of the non-FN behavior of the energy distribution from the (112) plane (Fig. 8). The dashed line in Fig. 15 is the projected enhancement factor. This effect is probably included in the Ba on tungsten curve for the (112) plane but is not large enough to alter the basic shape of that enhancement factor.

The triplet $^3P$ state of Ca is broader than the Ba triplet $^3D$ state, and is shifted upward more than the Ba state (Fig. 18). This is a direct consequence of the delocalization of a $p$-like state relative to a $d$ state. For the Ca triplet $^3P$ level $E_\varphi{}^{3P}\approx -3.9$ eV with $\Delta E^{3P}\approx 0.4$ eV and $\Gamma_3{}^P\approx 0.3$ eV. These values all lie between those obtained for $S$ and $D$ states for Ba, in agreement with expectations.

## IV. CONCLUSIONS

The measured energy dependence of the enhanced tunneling through single adsorbed atoms has been analyzed in terms of a physically appealing and computationally simple model by Gadzuk.[23] We have also extended the one-dimensional model calculation of DA[20] to physically more realistic cases in order to predict the effect of a given energy level on the energy distribution. Combining the tunneling-resonance theory[23] with the experimental enhancement factors yielded direct information concerning the lifetime broadening and energy shifts of the virtual surface-impurity state of alkaline-earth atoms adsorbed on a single-crystal tungsten surface. Thus from direct experimental information we have confirmed the following theoretical model of electropositive adsorption[14–16]: that the configuration of a single electropositive adsorbate on a metal surface at low temperatures can be represented by a broadened, shifted, and partially occupied virtual energy level. It may be convenient in interpreting some experimental results to talk about a two-state system (ion or neutral), but this is simply a model construct and must not be interpreted as meaning that the electropositive adsorbate exists in either one state of the other, determined by some statistical weighing function.

The data for Ba and Ca demonstrate clearly that the ground-state configuration of an adsorbed atom may be a mixture of the atomic ground state and excited atomic states due to the atom-metal interaction. In the case of the alkaline-earth adsorbates this results because the atomic ground state of these atoms is an $ns^2$ level which shifts and broadens more upon interaction with the surface than the excited states of higher angular momentum. The half-width and shift of the observed states in Ba and Ca decreased as the angular momentum of the state increased: $\Gamma_S>\Gamma_P>\Gamma_D$ and $\Delta E_S>\Delta E_P>\Delta E_D$, especially when the principal quantum number of the excited state is less than the ground state.

The nature of the atom-metal interaction depends upon the character and number of excited states below the Fermi surface. For example, if the energy

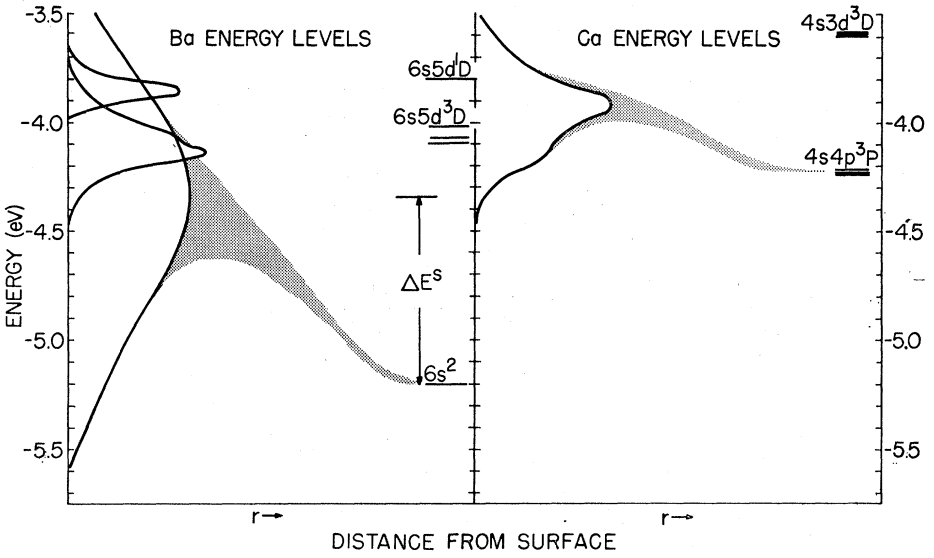


FIG. 18. Pictorial representation of the broadening and shifting of the energy levels of Ba and Ca as they interact with the surface. The shapes and position of the virtual levels at the surface are taken from the data on the low work-function planes of tungsten.

levels of Ba (see Fig. 18) were the same for different crystal faces of a given substrate metal with work functions which varied from 3.8 to 4.2 eV, then on the low work-function plane two $D$ levels would be below the Fermi surface, while on the high work-function face only an $S$ level would be below the Fermi surface. Obviously such quantities as the heat of adsorption or activation energy for diffusion will depend upon the number of levels below the Fermi surface.

Within the limitations of our field extrapolation scheme we can determine the effective charge on the adsorbed atom and its distance from the surface (plus the screening length). This would furnish an experimental check on the theoretical dipole moment calculations[17] and allow the theoretician to concentrate on the difficult problem of screening. A Ba atom on the (013), (111), and (112) planes of tungsten at zero field has a nearly half-filled "virtual level." From the field shift of the energy levels we obtain a dipole moment of $13\pm3$ D for Ba on the (013) and (111) planes of tungsten, in excellent agreement with Schmidt's[45] measurements.

Conceivably one could simultaneously observe the position and character of the energy levels of an adsorbed atom and then measure its binding energy for a given atom-metal configuration. Finally, a potentially very important observation of this study was the effect of band structure on the enhancement factors. Certain adsorbates seem to act as filters for or against the emission of electrons from tight-binding bands. This effect could be exploited in field-emission band-structure studies.

## ACKNOWLEDGMENTS

The authors would like to thank all the scientists in the Electron Physics Section of the National Bureau of Standards for the many useful discussions, especially Dr. C. J. Powell and Dr. C. E. Kuyatt, and H. Clark for his technical assistance. We are deeply indebted to Dr. J. W. Gadzuk for this theoretical guidance through this study. The evolution of this theoetical-experimental picture resulted from our day-to-day interchange with Dr. Gadzuk.